

Table 2. Clinical data of patients with NAFLD/NASH and chronic viral hepatitis.

	NAFLD/NASH	Chronic viral hepatitis
Age	51.2±2.0	56.7±2.8
Sex (male/female)	18/33	9/6
BMI	29.1±0.7	23.3±0.9**
AST (IU/L)	78.7±6.9	53.3±9.4
ALT (IU/L)	122.7±11.5	82.5±20.3

NAFLD, non-alcoholic fatty liver disease; NASH, non-alcoholic steatohepatitis; BMI, body mass index; AST, aspartate aminotransferase; ALT, alanine aminotransferase. Data are expressed as the mean ± SE. ***P*<0.01. doi:10.1371/journal.pone.0082163.t002

study. To the best of our knowledge, this is the first report to elucidate the potential role of hCLS in liver fibrosis in NASH. In our mouse model, the number of microgranulomas was quite low ($0.18 \pm 0.03/\text{mm}^2$) relative to that of hCLS ($25.61 \pm 0.18/\text{mm}^2$) (M. Itoh *et al.* unpublished observations). It is, therefore, technically difficult to examine the correlation of microgranulomas with the histological scores. On the other hand, the number of microgranuloma in the human biopsies was $3.67 \pm 0.35/\text{mm}^2$, which was much larger than that in MC4R-KO mice. This might be due to the difference in species or the degree of steatosis. In this regard, we do not exclude the possibility that microgranulomas are involved in liver fibrosis in human NASH. In line with this, there are several reports showing the increased number of microgranulomas in NASH relative to simple steatosis and the correlation between the number of microgranulomas and the extent of liver fibrosis [51,52]. Accordingly, it is interesting to know the difference of the role of hCLS and microgranulomas in liver fibrosis.

This study demonstrates for the first time that hCLS is a unique histological feature correlated with liver fibrosis in our mouse

model of NASH. We also observed increased number of hCLS in the liver of NAFLD/NASH patients. Our data suggest that in the development of NASH, macrophages constitute hCLS, where they interact with dead hepatocytes and fibrogenic cells, thereby accelerating inflammation and fibrosis in the liver. Collectively, our data provide evidence that hCLS is involved in the development of hepatic inflammation and fibrosis, thereby suggesting its pathophysiologic role in disease progression from simple steatosis to NASH.

Supporting Information

Figure S1 hCLS formation in mouse model of steatohepatitis. Sirius red (A) and F4/80 (B) stainings in the liver of MC4R-KO mice fed a high-fat diet (HFD) for 20 weeks. (C) Correlation of fibrosis area with hCLS number. Sirius red (D) and F4/80 (E) stainings in the liver from wildtype mice fed a HFD for one year. Sirius red (F) and F4/80 (G) stainings in the liver from wildtype mice fed a methionine and choline-deficient diet for 4 weeks. hCLS was indicated by arrows. Scale bars, 50 μm. (PDF)

Acknowledgments

The authors thank Dr. Joel K. Elmquist (University of Texas Southwestern Medical Center) for the generous gift of MC4R-KO mice and Dr. Jae Bum Kim (Seoul National University) for technical comment on immunohistochemistry. We also thank Ms. Kayoko Sakakibara for technical and secretarial assistances and the members of the Ogawa laboratory for helpful discussions.

Author Contributions

Conceived and designed the experiments: TS YO. Performed the experiments: MI HK KK HS SK MH TF KA. Analyzed the data: MI HK ST YK MT. Wrote the paper: MI HK ST TS YO. Clinical study: YM ST IS. Electron microscopic analysis: YK MT. Statistics: SA.

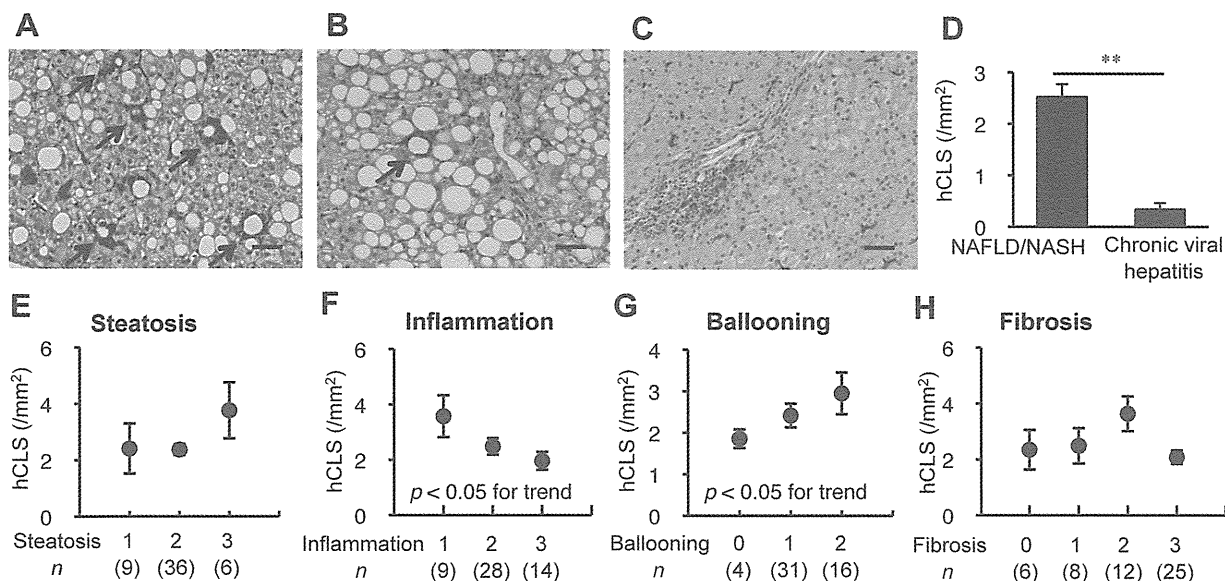


Figure 4. hCLS in human NASH. (A–C) Representative liver sections stained with CD68 antibody in patients with NASH (A), simple hepatic steatosis (B), and chronic viral hepatitis (C). Arrows indicate hCLS. (D) hCLS number in patients with NAFLD/NASH, and chronic viral hepatitis. Correlation of hCLS number with scores for hepatic steatosis (E), lobular inflammation (F), ballooning degeneration (G), and fibrosis stage (H) in patients with NAFLD/NASH. Scale bars, 50 μm. ** *P*<0.01. doi:10.1371/journal.pone.0082163.g004

References

- Anstee QM, Targher G, Day CP (2013) Progression of NAFLD to diabetes mellitus, cardiovascular disease or cirrhosis. *Nat Rev Gastroenterol Hepatol* 10: 330–344.
- Ratziu V, Bellentani S, Cortez-Pinto H, Day C, Marchesini G (2010) A position statement on NAFLD/NASH based on the EASL 2009 special conference. *J Hepatol* 53: 372–384.
- Adams LA, Lymp JF, St Sauver J, Sanderson SO, Lindor KD, et al. (2005) The natural history of nonalcoholic fatty liver disease: a population-based cohort study. *Gastroenterology* 129: 113–121.
- Marra F, Gastaldelli A, Sveglia Baroni G, Tell G, Tiribelli C (2008) Molecular basis and mechanisms of progression of non-alcoholic steatohepatitis. *Trends Mol Med* 14: 72–81.
- Day CP, James OF (1998) Steatohepatitis: a tale of two “hits”? *Gastroenterology* 114: 842–845.
- Browning JD, Horton JD (2004) Molecular mediators of hepatic steatosis and liver injury. *J Clin Invest* 114: 147–152.
- Neuschwander-Tetri BA (2010) Hepatic lipotoxicity and the pathogenesis of nonalcoholic steatohepatitis: the central role of nontriglyceride fatty acid metabolites. *Hepatology* 52: 774–788.
- Ramadori G, Armbrust T (2001) Cytokines in the liver. *Eur J Gastroenterol Hepatol* 13: 777–784.
- Rivera CA, Adegboye P, van Rooijen N, Tagalicud A, Allman M, et al. (2007) Toll-like receptor-4 signaling and Kupffer cells play pivotal roles in the pathogenesis of non-alcoholic steatohepatitis. *J Hepatol* 47: 571–579.
- Duffield JS, Forbes SJ, Constantinou CM, Clay S, Partolina M, et al. (2005) Selective depletion of macrophages reveals distinct, opposing roles during liver injury and repair. *J Clin Invest* 115: 56–65.
- Tosello-Trampont AC, Landes SG, Nguyen V, Novobrantseva TI, Hahn YS (2012) Kupffer cells trigger nonalcoholic steatohepatitis development in diet-induced mouse model through tumor necrosis factor- α production. *J Biol Chem* 287: 40161–40172.
- Varela-Rey M, Embade N, Ariz U, Lu SC, Mato JM, et al. (2009) Non-alcoholic steatohepatitis and animal models: understanding the human disease. *Int J Biochem Cell Biol* 41: 969–976.
- Itoh M, Suganami T, Nakagawa N, Tanaka M, Yamamoto Y, et al. (2011) Melanocortin 4 receptor-deficient mice as a novel mouse model of nonalcoholic steatohepatitis. *Am J Pathol* 179: 2454–2463.
- Suganami T, Tanaka M, Ogawa Y (2012) Adipose tissue inflammation and ectopic lipid accumulation. *Endocr J* 59: 849–857.
- Asano T, Watanabe K, Kubota N, Gunji T, Omata M, et al. (2009) Adiponectin knockout mice on high fat diet develop fibrosing steatohepatitis. *J Gastroenterol Hepatol* 24: 1669–1676.
- Kamada Y, Tamura S, Kiso S, Matsumoto H, Saji Y, et al. (2003) Enhanced carbon tetrachloride-induced liver fibrosis in mice lacking adiponectin. *Gastroenterology* 125: 1796–1807.
- Ikejima K, Takei Y, Honda H, Hirose M, Yoshikawa M, et al. (2002) Leptin receptor-mediated signaling regulates hepatic fibrogenesis and remodeling of extracellular matrix in the rat. *Gastroenterology* 122: 1399–1410.
- Imajo K, Fujita K, Yoneda M, Nozaki Y, Ogawa Y, et al. (2012) Hyperresponsivity to low-dose endotoxin during progression to nonalcoholic steatohepatitis is regulated by leptin-mediated signaling. *Cell Metab* 16: 44–54.
- Balthasar N, Dalgaard LT, Lee CE, Yu J, Funahashi H, et al. (2005) Divergence of melanocortin pathways in the control of food intake and energy expenditure. *Cell* 123: 493–505.
- Gautron L, Lee C, Funahashi H, Friedman J, Lee S, et al. (2010) Melanocortin-4 receptor expression in a vagal circuitry involved in postprandial functions. *J Comp Neurol* 518: 6–24.
- Nogueiras R, Wiedmer P, Perez-Tilve D, Veyrat-Durebex C, Keogh JM, et al. (2007) The central melanocortin system directly controls peripheral lipid metabolism. *J Clin Invest* 117: 3475–3488.
- Hotamisligil GS (2006) Inflammation and metabolic disorders. *Nature* 444: 860–867.
- Berg AH, Scherer PE (2005) Adipose tissue, inflammation, and cardiovascular disease. *Circ Res* 96: 939–949.
- Weisberg SP, McCann D, Desai M, Rosenbaum M, Leibel RL, et al. (2003) Obesity is associated with macrophage accumulation in adipose tissue. *J Clin Invest* 112: 1796–1808.
- Lumeng CN, Bodzin JL, Saltiel AR (2007) Obesity induces a phenotypic switch in adipose tissue macrophage polarization. *J Clin Invest* 117: 175–184.
- Lumeng CN, DelProposto JB, Westcott DJ, Saltiel AR (2008) Phenotypic switching of adipose tissue macrophages with obesity is generated by spatiotemporal differences in macrophage subtypes. *Diabetes* 57: 3239–3246.
- Cinti S, Mitchell G, Barbatelli G, Murano I, Ceresi E, et al. (2005) Adipocyte death defines macrophage localization and function in adipose tissue of obese mice and humans. *J Lipid Res* 46: 2347–2355.
- Apovian CM, Bigornia S, Mott M, Meyers MR, Ulloor J, et al. (2008) Adipose macrophage infiltration is associated with insulin resistance and vascular endothelial dysfunction in obese subjects. *Arterioscler Thromb Vasc Biol* 28: 1654–1659.
- Bremer AA, Devaraj S, Afify A, Jialal I (2011) Adipose tissue dysregulation in patients with metabolic syndrome. *J Clin Endocrinol Metab* 96: E1782–1788.
- Sakaida I, Terai S, Yamamoto N, Aoyama K, Ishikawa T, et al. (2004) Transplantation of bone marrow cells reduces CCl₄-induced liver fibrosis in mice. *Hepatology* 40: 1304–1311.
- Van Rooijen N, Sanders A (1994) Liposome mediated depletion of macrophages: mechanism of action, preparation of liposomes and applications. *J Immunol Methods* 174: 83–93.
- Itoh M, Suganami T, Satoh N, Tanimoto-Koyama K, Yuan X, et al. (2007) Increased adiponectin secretion by highly purified eicosapentaenoic acid in rodent models of obesity and human obese subjects. *Arterioscler Thromb Vasc Biol* 27: 1918–1925.
- Terai S, Ishikawa T, Omori K, Aoyama K, Marumoto Y, et al. (2006) Improved liver function in patients with liver cirrhosis after autologous bone marrow cell infusion therapy. *Stem Cells* 24: 2292–2298.
- Juluri R, Vuppalanchi R, Olson J, Unalp A, Van Natta ML, et al. (2010) Generalizability of the Nonalcoholic Steatohepatitis Clinical Research Network Histologic Scoring System for Nonalcoholic Fatty Liver Disease. *J Clin Gastroenterol* 45: 55–58.
- Magness ST, Bataller R, Yang L, Brenner DA (2004) A dual reporter gene transgenic mouse demonstrates heterogeneity in hepatic fibrogenic cell populations. *Hepatology* 40: 1151–1159.
- Cassiman D, Libbrecht L, Desmet V, Denef C, Roskams T (2002) Hepatic stellate cell/myofibroblast subpopulations in fibrotic human and rat livers. *J Hepatol* 36: 200–209.
- Zeisberg M, Yang C, Martino M, Duncan MB, Rieder F, et al. (2007) Fibroblasts derive from hepatocytes in liver fibrosis via epithelial to mesenchymal transition. *J Biol Chem* 282: 23337–23347.
- Ma KL, Ruan XZ, Powis SH, Chen Y, Moorhead JF, et al. (2008) Inflammatory stress exacerbates lipid accumulation in hepatic cells and fatty livers of apolipoprotein E knockout mice. *Hepatology* 48: 770–781.
- Miura K, Kodama Y, Inokuchi S, Schnabl B, Aoyama T, et al. (2010) Toll-like receptor 9 promotes steatohepatitis by induction of interleukin-1b in mice. *Gastroenterology* 139: 323–334 e327.
- Rivera CA, Bradford BU, Hunt KJ, Adachi Y, Schrum LW, et al. (2001) Attenuation of CCl₄-induced hepatic fibrosis by GdCl₃ treatment or dietary glycine. *Am J Physiol Gastrointest Liver Physiol* 281: G200–207.
- Thomas JA, Pope C, Wojtacha D, Robson AJ, Gordon-Walker TT, et al. (2011) Macrophage therapy for murine liver fibrosis recruits host effector cells improving fibrosis, regeneration, and function. *Hepatology* 53: 2003–2015.
- Iwamoto T, Terai S, Hisanaga T, Takami T, Yamamoto N, et al. (2013) Bone-marrow-derived cells cultured in serum-free medium reduce liver fibrosis and improve liver function in carbon-tetrachloride-treated cirrhotic mice. *Cell Tissue Res* 351: 487–495.
- Patsouris D, Li PP, Thapar D, Chapman J, Olefsky JM, et al. (2008) Ablation of CD11c-positive cells normalizes insulin sensitivity in obese insulin resistant animals. *Cell Metab* 8: 301–309.
- Medzhitov R (2008) Origin and physiological roles of inflammation. *Nature* 454: 428–435.
- Asanuma T, Ono M, Kubota K, Hirose A, Hayashi Y, et al. (2010) Super paramagnetic iron oxide MRI shows defective Kupffer cell uptake function in non-alcoholic fatty liver disease. *Gut* 59: 258–266.
- Rensen SS, Slaats Y, Nijhuis J, Jans A, Bieghs V, et al. (2009) Increased hepatic myeloperoxidase activity in obese subjects with nonalcoholic steatohepatitis. *Am J Pathol* 175: 1473–1482.
- Ioannou GN, Haigh WG, Thorning D, Savard C (2013) Hepatic cholesterol crystals and crown-like structures distinguish NASH from simple steatosis. *J Lipid Res* 54: 1326–1334.
- Brunt EM (2010) Pathology of nonalcoholic fatty liver disease. *Nat Rev Gastroenterol Hepatol* 7: 195–203.
- Tiniakos DG, Vos MB, Brunt EM (2010) Nonalcoholic fatty liver disease: pathology and pathogenesis. *Annu Rev Pathol* 5: 145–171.
- Kleiner DE (2006) Granulomas in the liver. *Semin Diagn Pathol* 23: 161–169.
- Caballero T, Gila A, Sanchez-Salgado G, Munoz de Rueda P, Leon J, et al. (2012) Histological and immunohistochemical assessment of liver biopsies in morbidly obese patients. *Histol Histopathol* 27: 459–466.
- Fotiadu A, Gagalis A, Akriviadis E, Kotoula V, Sinakos E, et al. (2010) Clinicopathological correlations in a series of adult patients with non-alcoholic fatty liver disease. *Pathol Int* 60: 87–92.

Yorihiro Iwasaki,^{1,4} Takayoshi Suganami,^{2,8} Rumi Hachiya,^{1,9} Ibuki Shirakawa,² Misa Kim-Saijo,¹ Miyako Tanaka,¹ Miho Hamaguchi,¹ Takako Takai-Igarashi,⁵ Michikazu Nakai,⁶ Yoshihiro Miyamoto,^{6,7} and Yoshihiro Ogawa^{1,3}

Activating Transcription Factor 4 Links Metabolic Stress to Interleukin-6 Expression in Macrophages



Chronic inflammation is a molecular element of the metabolic syndrome and type 2 diabetes. Saturated fatty acids (SFAs) are considered to be an important proinflammatory factor. However, it is still incompletely understood how SFAs induce proinflammatory cytokine expression. Hereby we report that activating transcription factor (ATF) 4, a transcription factor that is induced downstream of metabolic stresses including endoplasmic reticulum (ER) stress, plays critical roles in SFA-induced interleukin-6 (IL6) expression. DNA microarray analysis using primary macrophages revealed that the ATF4 pathway is activated by SFAs. Haploinsufficiency and short hairpin RNA-based knockdown of ATF4 in macrophages markedly

inhibited SFA- and metabolic stress-induced IL6 expression. Conversely, pharmacological activation of the ATF4 pathway and overexpression of ATF4 resulted in enhanced IL6 expression. Moreover, ATF4 acts in synergy with the Toll-like receptor-4 signaling pathway, which is known to be activated by SFAs. At a molecular level, we found that ATF4 exerts its proinflammatory effects through at least two different mechanisms: ATF4 is involved in SFA-induced nuclear factor- κ B activation; and ATF4 directly activates the IL6 promoter. These findings provide evidence suggesting that ATF4 links metabolic stress and IL6 expression in macrophages.

Diabetes 2014;63:152–161 | DOI: 10.2337/db13-0757

¹Department of Molecular Endocrinology and Metabolism, Graduate School of Medical and Dental Sciences, Tokyo Medical and Dental University, Tokyo, Japan

²Department of Organ Network and Metabolism, Graduate School of Medical and Dental Sciences, Tokyo Medical and Dental University, Tokyo, Japan

³Global Center of Excellence Program, International Research Center for Molecular Science in Tooth and Bone Diseases, Tokyo Medical and Dental University, Tokyo, Japan

⁴Center for Diabetes and Endocrinology, The Tazuke Kofukai Medical Research Institute, Kitano Hospital, Osaka, Japan

⁵Department of Health Record Informatics, Tohoku Medical Megabank Organization, Tohoku University, Miyagi, Japan

⁶Department of Preventive Medicine and Epidemiologic Informatics, National Cerebral and Cardiovascular Center, Osaka, Japan

⁷Department of Preventive Cardiology, National Cerebral and Cardiovascular Center, Osaka, Japan

⁸Precursory Research for Embryonic Science and Technology, Japan Science and Technology Agency, Tokyo, Japan

⁹Japan Society for the Promotion of Science for Young Scientists, Tokyo, Japan

Corresponding author: Takayoshi Suganami, suganami.mem@tmd.ac.jp, or Yoshihiro Ogawa, ogawa.mem@tmd.ac.jp.

Received 10 May 2013 and accepted 26 August 2013.

This article contains Supplementary Data online at <http://diabetes.diabetesjournals.org/lookup/suppl/doi:10.2337/db13-0757/-/DC1>.

© 2014 by the American Diabetes Association. See <http://creativecommons.org/licenses/by-nc-nd/3.0/> for details.

See accompanying commentary, p. 48.

Chronic inflammation is a molecular element of the metabolic syndrome and type 2 diabetes. Several proinflammatory signaling pathways, including interleukin 6 (IL-6) signaling, are shown to play essential roles in the pathophysiology of the metabolic syndrome, type 2 diabetes, and subsequent cardiovascular diseases (1–3). As a causative factor of chronic inflammation, several lines of evidence support the role of free fatty acids. Of note, saturated fatty acids (SFAs), such as palmitate (Pal) and stearate, have been shown to induce proinflammatory cytokine production in various cell types, including macrophages (4,5). However, the underlying mechanism of SFA-induced proinflammatory cytokine expression is only partially elucidated.

To date, we and others have demonstrated that Toll-like receptor-4 (TLR4), a pathogen sensor expressed on the cell surface, plays a critical role in the SFA-induced proinflammatory cytokine expression (4–6). On the other hand, multiple mechanisms are involved in the SFA-induced cellular responses (1,7,8). Among them, attention has been focused on the role of cellular metabolic stresses such as endoplasmic reticulum (ER) stress and oxidative stress (1). Recent reports suggest that the modulation of metabolic stress pathways may alter high-fat diet-induced proinflammatory cytokine expression as well as insulin resistance (9,10). Therefore, it is of importance to clarify the molecular mechanism by which metabolic stresses affect proinflammatory cytokine expression.

In this study, using DNA microarray and network analyses in macrophages, we show that activating transcription factor (ATF) 4, a basic leucine zipper transcription factor, is potentially induced by SFAs. We provide evidence that ATF4 plays essential roles in *Il6* expression induced by various metabolic stresses, including ER stress. Furthermore, the ATF4 pathway has a synergistic effect on the TLR4 signaling pathway, enhancing *Il6* expression. As a molecular mechanism, ATF4 is capable of enhancing metabolic stress-induced nuclear factor- κ B (NF- κ B) activation and directly activating the *Il6* promoter. Our data suggest that ATF4 is a novel link between metabolic stress and *Il6* expression in macrophages.

RESEARCH DESIGN AND METHODS

Mice, Cells, and Reagents

Tlr4- and *Atf4*-deficient mice were provided by Dr. Shizuo Akira (Osaka University, Osaka, Japan). Mice were maintained on the C57BL/6 (B6) genetic background. All animal experiments were performed in accordance with the guidelines of Tokyo Medical and Dental University (no. 2011–207C, no. 0130269A). Murine peritoneal and bone marrow-derived macrophages (BMDMs) were prepared as described (11). All primary cells used for in vitro experiments were on the B6 background. Splenic CD11b-positive cells were purified using anti-CD11b magnetic

beads and LS-columns (Miltenyi Biotec, Bergisch Gladbach, Germany). The RAW264 macrophage cell line (RIKEN BioResource Center, Tsukuba, Japan) was maintained in Dulbecco's modified Eagle's medium (Nacalai Tesque, Kyoto, Japan) containing 10% FBS. Palmitate (P5585), stearate (P4751), lipopolysaccharide (LPS; P4391), lipid A (L5399), and a double-stranded RNA-dependent protein kinase (PKR) inhibitor (2-aminopurine; A3509) were purchased from Sigma-Aldrich (St. Louis, MO). Fatty acids were solubilized in ethanol, and conjugated with fatty acid-free and Ig-free BSA at a molar ratio of 10:1 (fatty acid/albumin) in serum-poor medium (0.5% FBS) (4). The vehicle control used was a mixture of ethanol and BSA alone in place of fatty acids. A PKR-like ER kinase (PERK) inhibitor (GSK2606414) was obtained from EMD Millipore (Calbiochem; Billerica, MA). A stearyl-CoA desaturase 1 inhibitor (A939572) was from BioVision (Milpitas, CA). Antibodies against ATF4 (sc200), RelA (sc372), ATF3 (sc188), β -actin (sc47778), and Lamin A/C (sc20681) were from Santa Cruz Biotechnology (Dallas, TX). Antibodies against I κ B α (catalog #9242), eukaryotic initiation factor-2 α (eIF2 α ; catalog #9722), and phospho-eIF2 α (catalog #9721) were from Cell Signaling Technology (Danvers, MA). An antibody against ATF6 (IMG273) was from Imgenex (San Diego, CA).

Microarray, Network, and Pathway Analyses

Total RNAs were extracted from thioglycollate-elicited peritoneal macrophages using the RNeasyMini Kit (Qiagen, Valencia, CA). Microarray analysis was performed on biological duplicate samples using Affymetrix GeneChip Mouse Genome 430 2.0 Arrays according to the manufacturer's instructions (12). Genes with an average fold change >1.8 and labeled as both "present (P)" and "increased (I)" were considered to be differentially upregulated. Affymetrix probe IDs were converted to unique Entrez IDs. Protein networks were built running the Markov clustering algorithm using the functional and physical interaction scores from STRING 9.0 with an inflation parameter of 2.0. Markov clustering has been used by many groups to build protein complexes or families based on protein-protein interactions (13,14). The results were visualized in Cytoscape software (15). Pathway and gene ontology analyses were performed using the Reactome functional protein interaction database (<http://www.reactome.org/>).

Nuclear Cytoplasmic Fractionation

The cells were collected in ice-cold PBS, resuspended in buffer A (10 mmol/L HEPES-KOH at pH 7.8, 10 mmol/L KCl, 0.1 mmol/L EDTA, 1 mmol/L dithiothreitol, 0.5 mmol/L phenylmethylsulfonyl fluoride, and protease inhibitors) and incubated on ice for 5 min. The cells were then spun down, and the cytoplasmic fraction was aspirated to separate tubes. The nuclear fraction was then lysed in buffer C (50 mmol/L HEPES-KOH at pH 7.8,

420 mmol/L KCl, 0.1 mmol/L EDTA, 5 mmol/L MgCl₂, 1 mmol/L dithiothreitol, 0.5 mmol/L phenylmethylsulfonyl fluoride, and protease inhibitors) at 4°C for 30 min. The lysate was clarified by centrifugation, and the supernatant was collected.

Chromatin Immunoprecipitation Assay

Chromatin immunoprecipitation was performed using the MAGnify Chromatin Immunoprecipitation System (49–2024; Invitrogen, Carlsbad, CA) according to the manufacturer's instructions with some modifications. In brief, thioglycollate-elicited peritoneal macrophages were cross-linked with 1% (w/v) formaldehyde for 10 min and lysed in the buffer provided. Nuclear extracts from 3×10^6 to 1×10^7 cells were used per immunoprecipitation reaction. Sonicated nuclear extracts were immunoprecipitated for 2 h at 4°C with anti-ATF4 (sc200x, 3 μg), anti-RelA (sc372, 3 μg), or IgG isotype negative control (sc2027, 3 μg) antibodies (Santa Cruz Biotechnology). DNA was eluted and purified as previously described (16). Eluted DNA was quantified with quantitative PCR using SYBR GREEN chemistry (StepOne Plus; Applied Biosystems, Foster City, CA).

RNA Purification, Reverse Transcription, and Real-Time PCR Amplification

RNA was purified using Sepasol (30486–56; Nacalai Tesque), according to the manufacturer's instructions. Total RNA (1.25 μg) was reverse-transcribed using a ReverTraAce (FSQ-201; Toyobo, Osaka, Japan). Ten nanograms of cDNA were used for real-time PCR amplification with SYBR GREEN detection protocol in a thermal cycler (StepOne Plus; Applied Biosystems). Data were normalized to the 36B4 levels and analyzed using the comparative threshold cycle method (12). Primer sequences are listed in Supplementary Table 1.

Plasmid Construction, Transfection, and Knockdown Experiments

An expression vector encoding murine ATF4 was constructed by inserting PCR-amplified cDNA fragment encoding ATF4 between the *EcoRI* and *BamHI* sites of the pcDNA3.1Myc-His3 expression vector. For generation of the ATF4 5' untranslated region (UTR) luciferase reporter plasmid, the 285 base pairs of murine ATF4 5' UTR was amplified by PCR and was inserted into the *HindIII* site of the pGL3 control vector (E1741; Promega, Madison, WI). The rat *Il6* promoter luciferase reporter plasmid and various truncated constructs (17) were gifts from Dr. Toshihiro Ichiki (Kyushu University, Fukuoka, Japan). The *Il6* promoter construct containing mutant ATF/cAMP-responsive element-binding protein site was generated from the *Il6* promoter construct 2 by the inverse PCR-based site-directed mutagenesis using KOD plus DNA polymerase (KOD201; Toyobo). The thymidine-kinase promoter renilla luciferase reporter vector was purchased from Promega. All transfection experiments were performed using Lipofectamine LTX reagent

(A12621; Invitrogen) according to the manufacturer's protocol. Retrovirus-mediated knockdown of ATF4 was performed as previously described (18). The target sequences for short hairpin (sh) ATF4 were 5'-TCCCTCCATGTGTAAAGGA-3' (shATF4 1) and 5'-CTCTGTTTCGAATGGATGA-3' (shATF4 2), respectively. As a negative control, shGFP was used as described previously (18).

Luciferase Assay

For the ATF4 5' UTR luciferase assay, RAW264 macrophages seeded on 24-well plates were transiently cotransfected with 30 ng renilla and 600 ng firefly luciferase reporter plasmids. For the *Il6* promoter luciferase assay RAW264 macrophages were transiently cotransfected with 50 ng renilla and 250 ng firefly luciferase reporter plasmids. Twenty-four hours after transfection, cells were collected and luciferase activity was measured with a dual-luciferase reporter assay system (Promega) according to the manufacturer's protocol. All data were normalized for transfection efficiency by the division of firefly luciferase activity by renilla luciferase activity.

NF-κB RelA DNA-Binding Activity Assay

Ten micrograms of nuclear extracts was used to determine RelA (p65) DNA-binding activity using an ELISA-based assay (TransAM 40096; Active Motif, Carlsbad, CA), according to the manufacturer's instructions. In brief, κB oligonucleotide-coated plates (in a 96-well format) were incubated for 1 h with the nuclear extracts. Specificity was achieved by incubation with anti-RelA primary antibodies for 1 h. Horseradish peroxidase-conjugated secondary antibodies were used for the detection of RelA bound to the κB sequences.

ELISA

ELISA of mouse IL-6 was performed using Mouse IL-6 Quantikine ELISA Kit (R&D Systems, Minneapolis, MN), as described previously (19).

Statistical Analysis

Data were expressed as the mean ± SEM. *P* values were calculated using two-tailed Student *t* tests.

RESULTS

ATF4 Pathway Is Activated by SFAs in the Absence of TLR4

In an attempt to identify novel mechanisms underlying the SFA-induced inflammatory responses, we performed DNA microarray analysis of palmitate-stimulated peritoneal macrophages obtained from *Tlr4*-deficient and wild-type mice. A total of 122 genes were upregulated by palmitate in both *Tlr4*-deficient and wild-type macrophages (Fig. 1A). We next performed Markov clustering of these genes using STRING database (20), which produced several clusters (Fig. 1B). Pathway analysis using the Reactome database (21) identified two large clusters

©

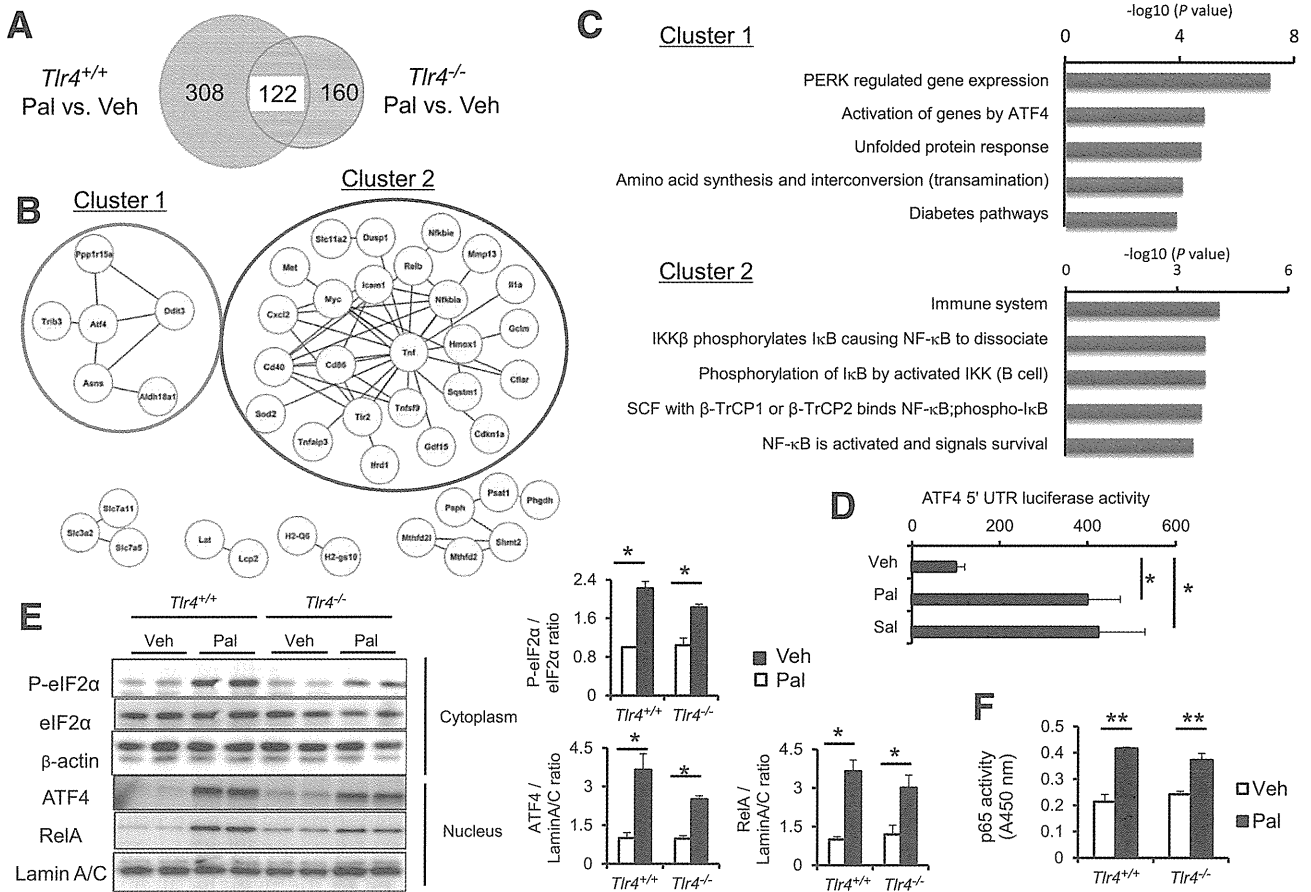


Figure 1—The ATF4 pathway is activated by SFAs in the absence of TLR4. **A**: Venn diagram showing genes induced by palmitate (Pal) in a TLR4-independent manner. *Tlr4*^{+/+} and *Tlr4*^{-/-} peritoneal macrophages were treated with 500 μ mol/L Pal or BSA (Veh) for 8 h. **B**: Network analysis of the 122 genes in the overlap in **A** on the STRING 9.0 database interaction network, followed by Markov clustering algorithm. **C**: Pathway analysis of the clusters formed in **B** using the Reactome database. **D**: Activation of ATF4 translation by Pal. RAW264 cells were transiently transfected with the ATF4 5' UTR luciferase construct. Cells were stimulated with 500 μ mol/L Pal, 20 μ mol/L Sal (used as a positive control) or Veh for 8 h ($*P < 0.05$, $n = 3$). **E**: Western blotting of cytoplasmic (for P-eIF2 α , eIF2 α , and β -actin) and nuclear (for ATF4, RelA, and lamin A/C) fractions of *Tlr4*^{+/+} and *Tlr4*^{-/-} peritoneal macrophages. Cells were stimulated with 500 μ mol/L Pal or Veh for 8 h. Representative blots (left) and quantitative results (right) are shown ($*P < 0.05$, $n = 5$). **F**: NF- κ B activity assay. *Tlr4*^{+/+} and *Tlr4*^{-/-} peritoneal macrophages were treated with 500 μ mol/L Pal or Veh for 4 h. NF- κ B p65/RelA activity in the nuclear extract was measured ($**P < 0.01$, $n = 3$). IKK, inhibitor of nuclear factor κ B kinase; I κ B, inhibitor of nuclear factor κ B; SCF, Skp1-cullin-F-box protein; β -TrCP, β -transducin repeat-containing protein.

in which target genes for ATF4 and NF- κ B were enriched (Fig. 1C). Indeed, several signaling pathways that can induce ATF4 were significantly enriched in gene ontology analysis (Supplementary Fig. 1).

ATF4 is induced following phosphorylation of eIF2 α , which is mediated by eIF2 α kinases (i.e., the heme-regulated eIF2 α kinase, PKR, PERK, and the general control nonderepressible 2) under metabolic stresses such as ER stress, oxidative stress, and amino acid deprivation (22). Previous reports showed that at least two of the eIF2 α kinases, PKR and PERK, are activated by SFAs (9,23). Consistently, pharmacological inhibitors of PKR and PERK suppressed palmitate-induced activation of the ATF4 pathway (Supplementary Fig. 2A and B), suggesting that PKR and PERK are likely to be involved in SFA-induced eIF2 α phosphorylation. When eIF2 α is phosphorylated, ATF4 translation is preferentially upregulated

through the characteristic upstream open reading frames in the 5' UTR (24). Using ATF4 5' UTR luciferase assay, we confirmed that ATF4 translation was activated by palmitate in RAW264 macrophage-like cell lines (Fig. 1D). In line with this, palmitate increased ATF4 protein levels and the expression of target genes, such as tribbles homolog-3 (*Trib3*) and *c/ebp* homologous protein (*Chop*, also known as *Ddit3*) (25), in peritoneal macrophages, at least in part, independent of TLR4 (Fig. 1E, and Supplementary Fig. 2D). We also observed that other branches of the unfolded protein response were activated by palmitate in the absence of TLR4 (Supplementary Fig. 2C and D). Intriguingly, we found that, even in *Tlr4*-deficient macrophages, palmitate increased the expression of some proinflammatory cytokines, such as *Il6* and tumor necrosis factor (*Tnf*), to a lesser extent than wild-type macrophages (Supplementary Fig. 2D). Consistent

with this, nuclear protein levels and activity of RelA (p65), a transcriptional activating subunit of NF- κ B, were increased by palmitate in both wild-type and *Tlr4*-deficient macrophages (Fig. 1E and F). These results suggest that the ATF4 pathway, as well as the NF- κ B pathway, is activated in macrophages by palmitate in the absence of TLR4.

In addition, we confirmed that stearate, another SFA, also activated the ATF4 pathway in RAW264 macrophages (Supplementary Fig. 3A). By contrast, unsaturated fatty acids such as oleate and eicosapentaenoic acid did not activate the ATF4 pathway (Supplementary Fig. 3B). Notably, eicosapentaenoic acid effectively suppressed palmitate-induced activation of the ATF4 pathway (Supplementary Fig. 3B). We also found that pharmacological inhibition of fatty acid desaturation resulted in upregulation of ATF4 target genes (Supplementary Fig. 3C) (26,27), suggesting that intracellular

SFAs, not unsaturated fatty acids, play a role in the ATF4 pathway activation. Although further studies are required, our results are consistent with previous reports showing that altered membrane lipid composition may activate unfolded protein response pathways through several mechanisms, including calcium depletion (28) and direct activation of ER membrane sensors (29).

ATF4 Is Required for *Il6* Expression in Response to Metabolic Stresses

In contrast to NF- κ B (30), the role of ATF4 in the inflammatory pathway is not yet fully characterized. Because *Atf4*-null mice are mostly embryonic or neonatal lethal (31), in this study we used primary macrophages obtained from *Atf4*-haploinsufficient mice. We found that BMDMs from *Atf4*-haploinsufficient mice were defective in palmitate-induced mRNA expression of *Il6* (Fig. 2A). *Tnf* expression was only marginally attenuated

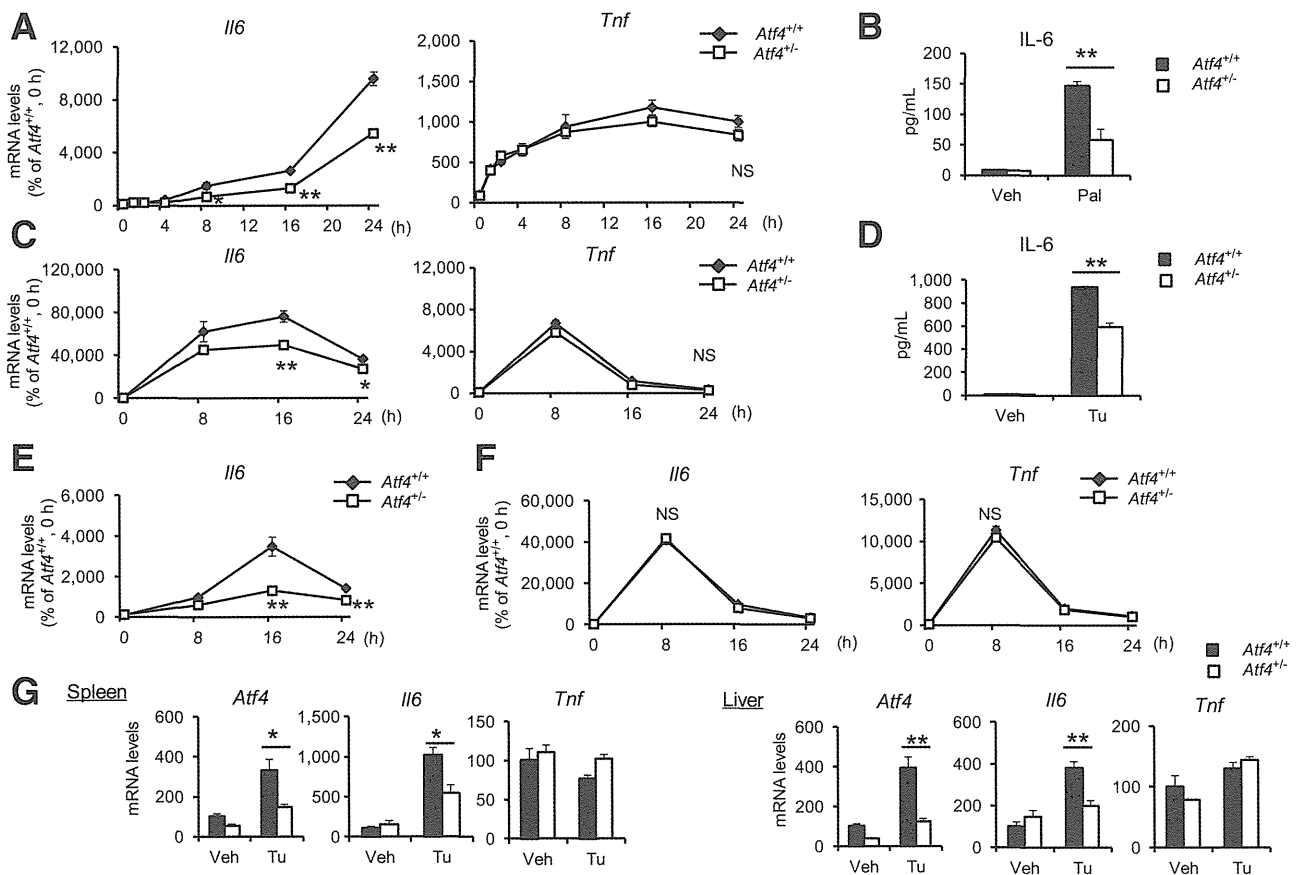


Figure 2—ATF4 is required for *Il6* expression in response to metabolic stresses. *A* and *B*: *Atf4*^{+/+} and *Atf4*^{+/-} BMDMs were treated with 500 μ M/L palmitate (Pal) or BSA (Veh). *A*: Expression levels of proinflammatory cytokines at the indicated time points (* P < 0.05, ** P < 0.01, n = 3). *B*: IL-6 levels in the culture media obtained from 24-h treated samples (** P = 0.0094, n = 3). *C* and *D*: *Atf4*^{+/+} and *Atf4*^{+/-} peritoneal macrophages were treated with 1 μ g/mL tunicamycin (Tu) or DMSO (Veh). *C*: Expression levels of proinflammatory cytokines at the indicated time points (* P < 0.05, ** P < 0.01, n = 3). *D*: IL-6 levels in the culture media obtained from 24-h treated samples (** P = 0.0006, n = 3). *E* and *F*: Expression levels of proinflammatory cytokines were measured at the indicated time points. *E*: *Atf4*^{+/+} and *Atf4*^{+/-} peritoneal macrophages were treated with 1 μ M thapsigargin (** P < 0.01, n = 3). *F*: *Atf4*^{+/+} and *Atf4*^{+/-} peritoneal macrophages were treated with 10 ng/mL lipid A (n = 3). *G*: *Atf4*^{+/+} and *Atf4*^{+/-} mice were intraperitoneally injected with Tu 1 mg/kg or DMSO (Veh). Sixteen hours after injection, expression levels of *Atf4* and proinflammatory cytokines were examined in the spleen and the liver (* P < 0.05, ** P < 0.01, n = 5).

in *Atf4*-haploinsufficient macrophages. Consistently, *Atf4*-haploinsufficient macrophages showed decreased secretion of IL-6 in the media (Fig. 2B). Similarly, *Atf4*-haploinsufficient peritoneal macrophages showed attenuated *Il6* expression induced by ER stressors, such as tunicamycin (Fig. 2C and D) and thapsigargin (Fig. 2E), compared with wild-type macrophages. To test the importance of ATF4 in RAW264 macrophages, we knocked down *Atf4*, which was confirmed by quantitative PCR and Western blotting (Supplementary Fig. 4A and B). *Atf4*

knockdown reduced SFA-induced (Supplementary Fig. 4C) or ER stress-induced (Supplementary Fig. 4D) *Il6* expression. On the other hand, in macrophages treated without these stressors, there was no significant difference in lipid A (a bona fide TLR4 ligand)-induced proinflammatory cytokine expression between the genotypes (Fig. 2F). To test the in vivo functional role of ATF4, we activated the ATF4 pathway by intraperitoneal injection of tunicamycin (Fig. 2G). Sixteen hours after the injection, tunicamycin treatment potently induced

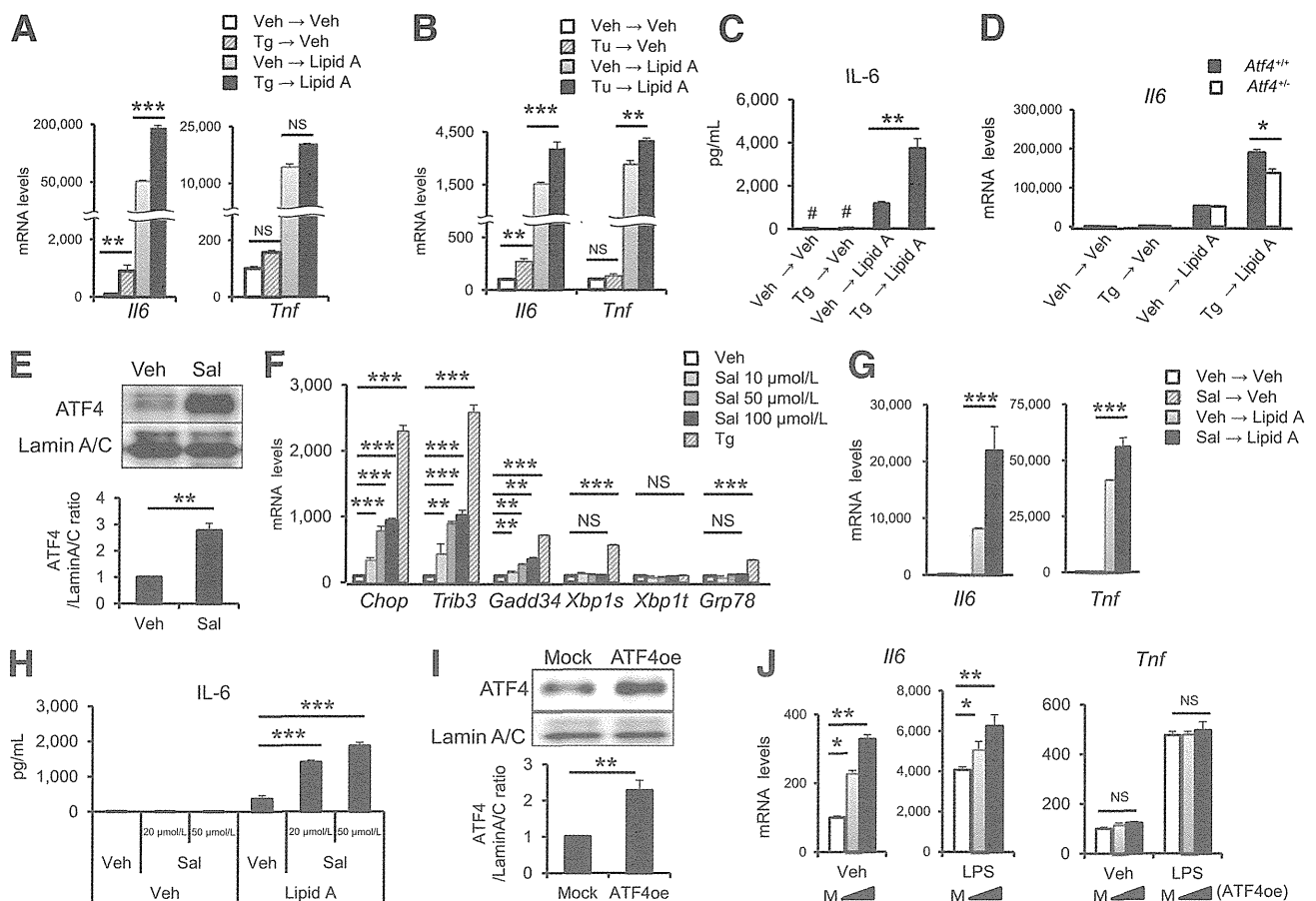


Figure 3—Activation of the ATF4 pathway exaggerates *Il6* expression in synergy with the TLR4 pathway. **A** and **B**: Expression levels of proinflammatory cytokines were measured. **A**: BMDMs were pretreated with 1 $\mu\text{mol/L}$ thapsigargin (Tg) or DMSO (Veh) for 2 h, then stimulated with 10 ng/mL lipid A or PBS (Veh) for 4 h ($^{**}P < 0.01$, $^{***}P < 0.001$, $n = 3$). **B**: Peritoneal macrophages were pretreated with 1 ng/mL tunicamycin (Tu) or DMSO (Veh) for 2 h, then stimulated with 10 ng/mL lipid A or PBS (Veh) for 4 h ($^{**}P < 0.01$, $^{***}P < 0.001$, $n = 3$). **C**: RAW264 macrophages were pretreated with 0.3 $\mu\text{mol/L}$ Tg or DMSO (Veh) for 2 h, then stimulated with 10 ng/mL lipid A or PBS (Veh) for 4 h. IL-6 levels in the culture media were measured by ELISA ($^{**}P = 0.0017$, $n = 4$; #below the lower limit of quantification). **D**: *Atf4*^{+/+} and *Atf4*^{+/-} BMDMs were pretreated with 1 $\mu\text{mol/L}$ Tg or DMSO (Veh) for 2 h, then stimulated with 10 ng/mL lipid A or PBS (Veh) for 4 h. Expression levels of proinflammatory cytokines were measured ($^{*}P = 0.0182$, $n = 3$). **E**: RAW264 macrophages were treated with 20 $\mu\text{mol/L}$ Sal or DMSO (Veh) for 4 h. ATF4 protein levels in the nucleus were determined by Western blotting. Representative blots (top) and quantitative results (bottom) are shown ($^{**}P < 0.01$, $n = 4$). **F** and **G**: Expression levels of proinflammatory cytokines were measured. **F**: RAW264 macrophages were treated with Sal (10, 50, 100 $\mu\text{mol/L}$) or 1 $\mu\text{mol/L}$ Tg or DMSO (Veh) for 4 h ($^{**}P < 0.01$, $^{***}P < 0.001$, $n = 3$). **G**: BMDMs were pretreated with 50 $\mu\text{mol/L}$ Sal or DMSO (Veh) for 4 h, then stimulated with 10 ng/mL lipid A or PBS (Veh) for 4 h ($^{**}P < 0.001$, $n = 3$). **H**: BMDMs were pretreated with Sal 20 and 50 $\mu\text{mol/L}$ or DMSO (Veh) for 4 h, then stimulated with 10 ng/mL lipid A or PBS (Veh) for 4 h. IL-6 levels in the culture media were measured ($^{***}P < 0.001$, $n = 3$). **I** and **J**: RAW264 macrophages were transiently transfected with expression vectors encoding murine ATF4 (ATF4oe) or empty vectors (Mock or M). **I**: Twenty-four hours after transfection, ATF4 protein levels in the nucleus were determined by Western blotting. Representative blots (top) and quantitative results (bottom) are shown ($^{**}P < 0.01$, $n = 4$). **J**: Twenty-four hours after transfection, cells were stimulated with 100 ng/mL LPS or PBS (Veh) for 4 h. Expression levels of proinflammatory cytokines were measured ($^{*}P < 0.05$, $^{**}P < 0.01$, $n = 3$). *Gadd34*, growth arrest and DNA damage-inducible gene 34; *Grp78*, glucose-regulated protein 78.

Atf4 and *Il6* mRNA expression in the spleen and liver from wild-type mice, which was significantly decreased in those from *Atf4*-haploinsufficient mice. *Tnf* expression was not significantly decreased. We obtained a similar result using purified CD11b-positive splenic macrophages (Supplementary Fig. 5). In this study, we observed no apparent difference in LPS-induced *Il6* mRNA expression between the genotypes (data not shown). These observations suggest that ATF4 plays a critical role in the metabolic stress-induced proinflammatory cytokine expression in vitro and in vivo.

ATF4 Pathway Enhances *Il6* Expression in Synergy With the TLR4 Pathway

We next examined the impact of the ATF4 pathway activation on proinflammatory cytokine expression in cells under metabolic stresses. Pretreatment of various

macrophages with ER stressors markedly enhanced the lipid A-induced mRNA expression and secretion of IL-6 (Fig. 3A–C and Supplementary Fig. 6A). The expression levels of *Tnf* were also affected to a lesser extent (Fig. 3A and B). Similar results were obtained using murine embryonic fibroblasts (MEFs) (Supplementary Fig. 6C). Although the magnitude varied, the patterns of gene expression in response to ER stressors and TLR4 agonists were similar among cell types. Notably, this enhancement was significantly attenuated in *Atf4*-haploinsufficient macrophages (Fig. 3D), ATF4 knockdown RAW264 macrophages (Supplementary Fig. 6B), and *Atf4*-deficient MEFs (Supplementary Fig. 6C). These observations suggest that the ATF4 pathway has a synergistic effect on the TLR4 signaling pathway.

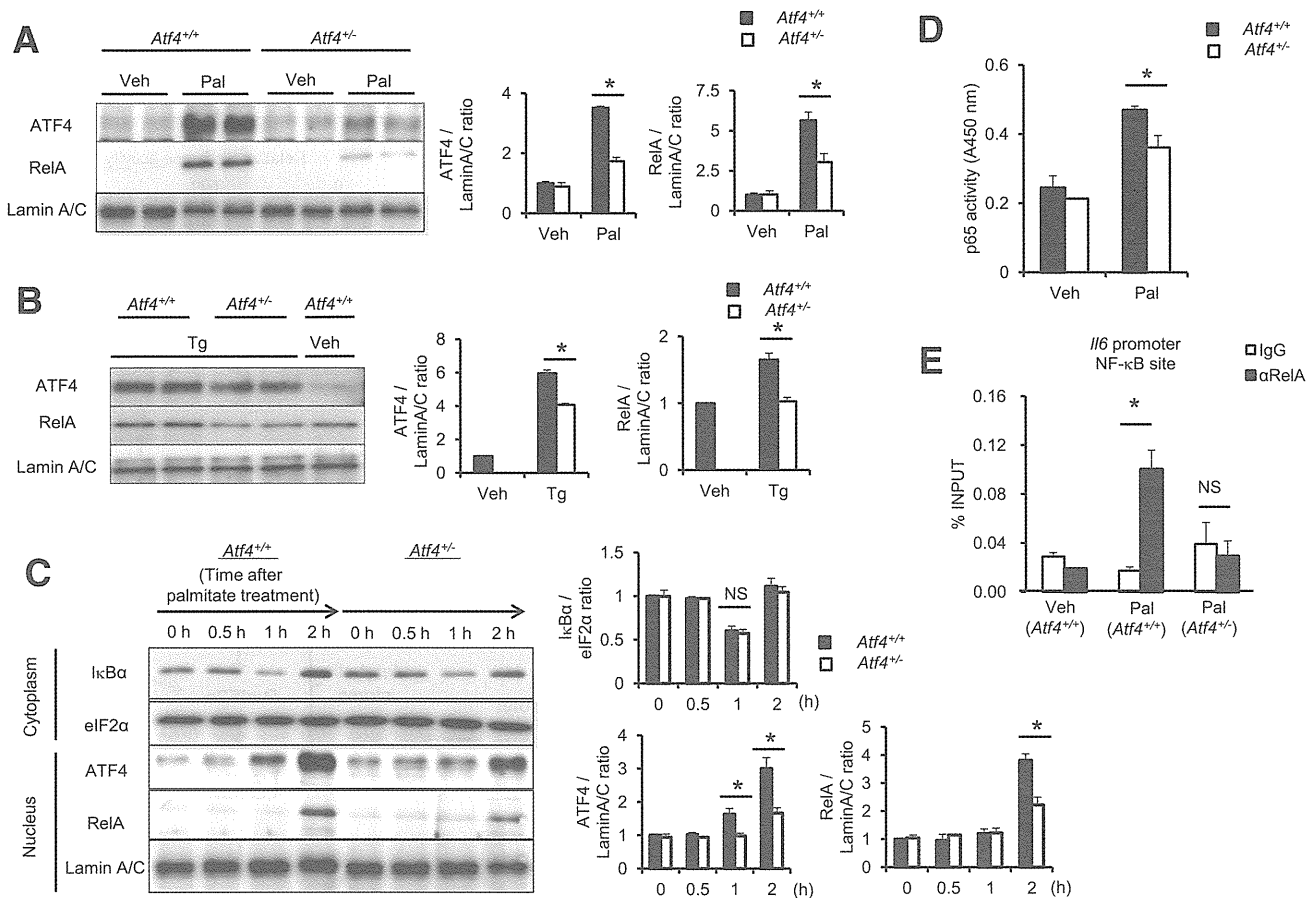


Figure 4—ATF4 is involved in NF- κ B activation in response to metabolic stresses. *A* and *B*: Western blotting of nuclear extracts from peritoneal macrophages. Representative blots (*left*) and quantitative results (*right*) are shown ($*P < 0.05$, $n = 4$ –5). *A*: Cells were treated with 500 μ M palmitate (Pal) or BSA (Veh) for 6 h. *B*: Cells were treated with 1 μ M thapsigargin (Tg) or DMSO (Veh) for 2 h. *C*: Earlier kinetics of Pal-induced changes in the NF- κ B pathway. Western blotting of cytoplasmic (for I κ B α and eIF2 α) and nuclear (for ATF4, RelA, and lamin A/C) fractions from peritoneal macrophages treated with 500 μ M Pal for indicated times. Representative blots (*left*) and quantitative results (*right*) are shown ($*P < 0.05$, $n = 4$). *D*: NF- κ B activity assay. *Atf4*^{+/+} and *Atf4*^{+/-} peritoneal macrophages were treated with 500 μ M Pal or BSA (Veh) for 4 h. NF- κ B p65/RelA activity in the nuclear extract was measured ($*P = 0.0295$, $n = 3$). *E*: A chromatin immunoprecipitation assay using *Atf4*^{+/+} and *Atf4*^{+/-} peritoneal macrophages. Cells were treated with 500 μ M Pal or BSA (Veh) for 4 h ($*P = 0.0349$, $n = 3$). Chromatin was immunoprecipitated and quantitated by PCR analysis of the region neighboring an NF- κ B site on the *Il6* promoter. I κ B α , inhibitor of nuclear factor κ B α .

In addition to the eIF2 α -ATF4 branch, ER stress activates two other branches of the unfolded protein response: the inositol requiring enzyme 1 α X-box binding protein 1 (XBP1) and ATF6 branches, the former of which is also involved in proinflammatory cytokine expression (32). To specifically stimulate the ATF4 pathway, we used salubrinal (Sal), an inhibitor of eIF2 α phosphatase complex (33). Pretreatment of BMDMs with Sal resulted in upregulation of ATF4 (Fig. 3E) and its target genes, whereas its effect on XBP1 splicing was minimal (Fig. 3F). Moreover, pretreatment with Sal potently enhanced the lipid A-induced mRNA expression and secretion of IL-6 in BMDMs (Fig. 3G and H) and RAW264 macrophages (Supplementary Fig. 6D and E). We also examined the effect of amino acid deprivation, another metabolic stress known to activate the ATF4 pathway (34), on *Il6* expression. Pretreatment with azetidine, a proline analog, significantly enhanced the lipid A-induced *Il6* expression (Supplementary Fig. 6F). Transient overexpression of ATF4 showed similar effects in RAW264 macrophages (Fig. 3I and J). These observations confirm that, in addition to the previously

characterized XBP1 pathway, the ATF4 pathway is also involved in the regulation of metabolic stress-induced proinflammatory cytokine expression. Of note, a recent report showed that the ATF4 pathway was attenuated following the low-dose treatment of TLR4 ligands in cultured macrophages (34). Collectively, it is conceivable that there is a bidirectional crosstalk between the ATF4 and TLR4 pathways.

ATF4 Is Involved in NF- κ B Activation in Response to Metabolic Stresses

We next aimed to clarify the molecular mechanism of the SFA-induced *Il6* expression through the ATF4 pathway. First, we examined the effect of ATF4 on palmitate-induced NF- κ B activation, because our microarray analysis revealed that the NF- κ B pathway was activated in *Tlr4*-deficient macrophages (Fig. 1B and C). In this study, we found that the nuclear protein levels and activity of RelA were increased by palmitate even in the absence of TLR4 (Fig. 1E and F). Interestingly, *Atf4* haploinsufficiency markedly reduced nuclear protein levels of RelA induced by palmitate or thapsigargin in peritoneal macrophages

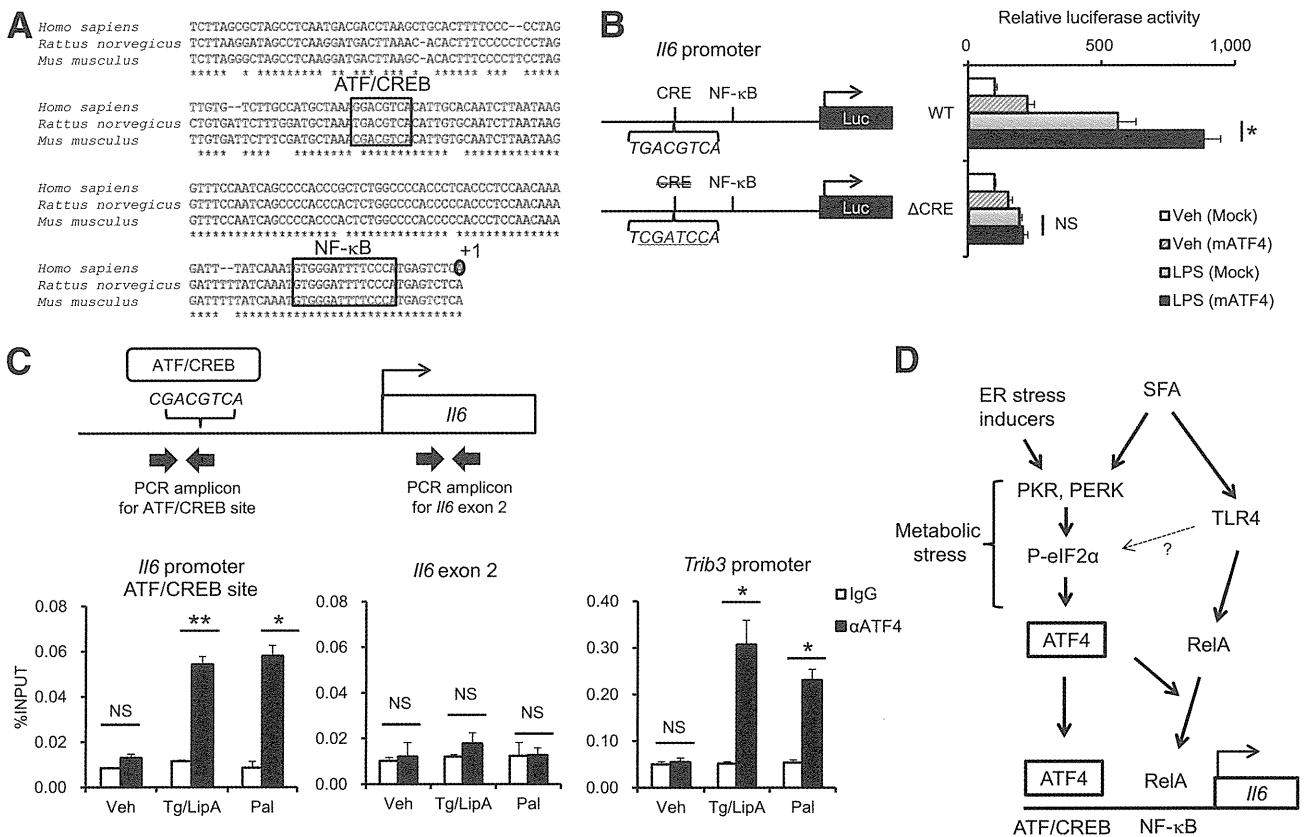


Figure 5—ATF4 directly activates the *Il6* promoter. **A**: The evolutionarily conserved region of the *Il6* promoter. **B**: The *Il6* promoter luciferase (Luc) assay in RAW264 macrophages. Cells were transiently transfected with expression vectors encoding murine ATF4 (mATF4) or empty vectors (Mock). Twenty-four hours after transfection, cells were stimulated with 100 ng/mL LPS for 24 h (**P* = 0.0154, *n* = 3). **C**: A chromatin immunoprecipitation assay using peritoneal macrophages. Cells were treated with BSA for 4 h (Veh), palmitate (Pal) (500 μ mol/L) for 4 h, or thapsigargin (Tg) (1 μ mol/L) for 2 h followed by lipid A (LipA) (10 ng/mL) for 4 h (**P* < 0.05, ***P* < 0.01, *n* = 3). Chromatin was immunoprecipitated and quantitated by PCR analysis of the region containing the ATF/CREB site on the *Il6* promoter. *Il6* exon 2 and the *Trib3* promoter were used as negative and positive control loci, respectively. **D**: Schematic representation. WT, wild type.

(Fig. 4A and B). We next examined the kinetics of cytoplasmic I κ B α degradation, a well-recognized event prior to nuclear translocation of RelA (30), and found no apparent difference in cytoplasmic I κ B α protein levels between the genotypes (Fig. 4C). Moreover, we observed that NF- κ B activity induced by palmitate was significantly attenuated in *Atf4*-haploinsufficient macrophages relative to wild-type macrophages (Fig. 4D). Consistently, a chromatin immunoprecipitation assay showed decreased recruitment of RelA to the *Il6* promoter region in *Atf4*-haploinsufficient macrophages (Fig. 4E). Because the transcriptional activity of RelA can be regulated by multiple mechanisms (30), further studies are required to elucidate how ATF4 affects RelA activity. Although a previous report showed that phosphorylation of eIF2 α leads to NF- κ B activation in MEFs (35), our data provide novel evidence that ATF4 is involved in metabolic stress-induced NF- κ B activation in macrophages.

ATF4 Directly Activates the *Il6* Promoter

On the basis of its potent proinflammatory effect, we next examined whether ATF4 directly activates *Il6* transcription. The consensus binding sequence of ATF4 is identical to that of the cAMP response element (CRE) (36). The *Il6* promoter contains an evolutionarily conserved region in which a putative ATF4-binding sequence is located in the vicinity of the NF- κ B-binding site (Fig. 5A). We, therefore, performed the *Il6* promoter luciferase assay using RAW264 macrophages. The luciferase activity was increased by treatment with LPS, which was further enhanced by ATF4 overexpression (Fig. 5B). The effect of ATF4 overexpression was abolished when transfected with the promoter construct containing a mutant CRE. Interestingly, the mutation in the CRE also markedly inhibited the LPS-induced activation of the *Il6* promoter. Consistently, experiments with a series of truncated *Il6* promoter constructs showed marked reduction of the promoter activity in the absence of CRE (Supplementary Fig. 5), suggesting that the CRE is indispensable for the LPS- and ATF4-induced activation of the *Il6* promoter. To confirm the direct recruitment of ATF4 to the *Il6* promoter region, we performed a chromatin immunoprecipitation assay using peritoneal macrophages. Signals from the promoter region containing the CRE were significantly increased upon treatment with palmitate or thapsigargin plus lipid A (Fig. 5C). These data suggest that ATF4 directly activates the *Il6* promoter.

DISCUSSION

In this study, we demonstrated that ATF4 is induced downstream of metabolic stresses caused by SFAs and ER stressors. ATF4 exerts its proinflammatory effects through at least two different mechanisms: direct activation of the *Il6* promoter and involvement in NF- κ B activation (Fig. 5D). According to previous reports, other members of ATF/CREB family of transcription factors are also involved in positive (e.g., XBP1) or negative

(e.g., ATF3) regulation of *Il6* expression (18,32). Of note, these factors may be induced downstream of TLR4 stimulation even independent of ER stress (18,32). By contrast, our results suggest that ATF4 is minimally involved in the TLR4 signaling in unstressed cells. Considering that the ATF4 pathway is activated under a variety of metabolic stresses, ATF4 would constitute a critical link between metabolic stresses and *Il6* expression.

Furthermore, our observations that the ATF4 pathway acts in synergy with the TLR4 pathway raise a possibility that metabolic stresses affect innate immune response. Consistent with several previous reports (4–6), our results suggest that TLR4 is required for proinflammatory effects of SFAs. Importantly, the current study also identifies the ATF4 pathway as a novel mechanism of SFA-induced proinflammatory cytokine expression that is induced even in the absence of TLR4. Given that SFAs activate both TLR4 and various metabolic stress pathways upstream of ATF4 (1,4–9), the cross talk between these pathways would be important for better understanding of the molecular mechanism of SFA-induced proinflammatory cytokine expression. Collectively, our findings raise the possibility that ATF4 plays a role in the pathophysiology of chronic inflammation in the metabolic syndrome and type 2 diabetes.

Acknowledgments. The authors thank Dr. Shizuo Akira, Osaka University, for providing *Atf4* haploinsufficient mice; Dr. Toshihiro Ichiki, Kyushu University, for providing *Il6* promoter luciferase plasmids; and Dr. Takahisa Nakamura, Cincinnati Children's Hospital Medical Center, for critical reading of the manuscript.

Funding. This work was supported in part by Grants-in-Aid for Scientific Research from the Ministry of Education, Culture, Sports, Science and Technology of Japan; Japan Science and Technology Agency, Precursory Research for Embryonic Science and Technology; Astellas Foundation for Research on Metabolic Disorders; and Nestlé Nutrition Council, Japan.

Duality of Interest. No potential conflicts of interest relevant to this article were reported.

Author Contributions. Y.I. and T.S. researched data, contributed to the discussion, and wrote, reviewed, and edited the manuscript. R.H., M.K.-S., M.T., and M.H. contributed to the discussion. I.S. researched data and contributed to the discussion. T.T.-I. contributed to network and pathway analyses. M.N. and Y.M. performed the microarray experiments. Y.O. contributed to the discussion and wrote, reviewed, and edited the manuscript. T.S. and Y.O. are the guarantors of this work and, as such, had full access to all the data in the study and take responsibility for the integrity of the data and the accuracy of the data analysis.

References

- Hotamisligil GS. Endoplasmic reticulum stress and the inflammatory basis of metabolic disease. *Cell* 2010;140:900–917
- Odegaard JI, Chawla A. Pleiotropic actions of insulin resistance and inflammation in metabolic homeostasis. *Science* 2013;339:172–177
- Osborn O, Olefsky JM. The cellular and signaling networks linking the immune system and metabolism in disease. *Nat Med* 2012;18:363–374
- Suganami T, Tanimoto-Koyama K, Nishida J, et al. Role of the Toll-like receptor 4/NF- κ B pathway in saturated fatty acid-induced

- inflammatory changes in the interaction between adipocytes and macrophages. *Arterioscler Thromb Vasc Biol* 2007;27:84–91
5. Shi H, Kokoeva MV, Inouye K, Tzameli I, Yin H, Flier JS. TLR4 links innate immunity and fatty acid-induced insulin resistance. *J Clin Invest* 2006;116:3015–3025
 6. Lee JY, Sohn KH, Rhee SH, Hwang D. Saturated fatty acids, but not unsaturated fatty acids, induce the expression of cyclooxygenase-2 mediated through Toll-like receptor 4. *J Biol Chem* 2001;276:16683–16689
 7. Erbay E, Babaev VR, Mayers JR, et al. Reducing endoplasmic reticulum stress through a macrophage lipid chaperone alleviates atherosclerosis. *Nat Med* 2009;15:1383–1391
 8. Holland WL, Bikman BT, Wang LP, et al. Lipid-induced insulin resistance mediated by the proinflammatory receptor TLR4 requires saturated fatty acid-induced ceramide biosynthesis in mice. *J Clin Invest* 2011;121:1858–1870
 9. Nakamura T, Furuhashi M, Li P, et al. Double-stranded RNA-dependent protein kinase links pathogen sensing with stress and metabolic homeostasis. *Cell* 2010;140:338–348
 10. Ozcan U, Yilmaz E, Ozcan L, et al. Chemical chaperones reduce ER stress and restore glucose homeostasis in a mouse model of type 2 diabetes. *Science* 2006;313:1137–1140
 11. Suganami T, Nishida J, Ogawa Y. A paracrine loop between adipocytes and macrophages aggravates inflammatory changes: role of free fatty acids and tumor necrosis factor alpha. *Arterioscler Thromb Vasc Biol* 2005;25:2062–2068
 12. Ichioka M, Suganami T, Tsuda N, et al. Increased expression of macrophage-inducible C-type lectin in adipose tissue of obese mice and humans. *Diabetes* 2011;60:819–826
 13. Krogan NJ, Cagney G, Yu H, et al. Global landscape of protein complexes in the yeast *Saccharomyces cerevisiae*. *Nature* 2006;440:637–643
 14. Bergholdt R, Brorsson C, Lage K, Nielsen JH, Brunak S, Pociot F. Expression profiling of human genetic and protein interaction networks in type 1 diabetes. *PLoS One* 2009;4:e6250
 15. Shannon P, Markiel A, Ozier O, et al. Cytoscape: a software environment for integrated models of biomolecular interaction networks. *Genome Res* 2003;13:2498–2504
 16. Dahl JA, Collas P. A rapid micro chromatin immunoprecipitation assay (microChIP). *Nat Protoc* 2008;3:1032–1045
 17. Tian Q, Miyazaki R, Ichiki T, et al. Inhibition of tumor necrosis factor- α -induced interleukin-6 expression by telmisartan through cross-talk of peroxisome proliferator-activated receptor- γ with nuclear factor κ B and CCAAT/enhancer-binding protein- β . *Hypertension* 2009;53:798–804
 18. Suganami T, Yuan X, Shimoda Y, et al. Activating transcription factor 3 constitutes a negative feedback mechanism that attenuates saturated fatty acid/Toll-like receptor 4 signaling and macrophage activation in obese adipose tissue. *Circ Res* 2009;105:25–32
 19. Itoh M, Suganami T, Nakagawa N, et al. Melanocortin 4 receptor-deficient mice as a novel mouse model of nonalcoholic steatohepatitis. *Am J Pathol* 2011;179:2454–2463
 20. Szklarczyk D, Franceschini A, Kuhn M, et al. The STRING database in 2011: functional interaction networks of proteins, globally integrated and scored. *Nucleic Acids Res* 2011;39(Database issue):D561–D568
 21. Joshi-Tope G, Gillespie M, Vastrik I, et al. Reactome: a knowledgebase of biological pathways. *Nucleic Acids Res* 2005;33(Database issue):D428–D432
 22. Harding HP, Zhang Y, Zeng H, et al. An integrated stress response regulates amino acid metabolism and resistance to oxidative stress. *Mol Cell* 2003;11:619–633
 23. Ishiyama J, Taguchi R, Akasaka Y, et al. Unsaturated FAs prevent palmitate-induced LOX-1 induction via inhibition of ER stress in macrophages. *J Lipid Res* 2011;52:299–307
 24. Vattem KM, Wek RC. Reinitiation involving upstream ORFs regulates ATF4 mRNA translation in mammalian cells. *Proc Natl Acad Sci USA* 2004;101:11269–11274
 25. Ohoka N, Yoshii S, Hattori T, Onozaki K, Hayashi H. TRB3, a novel ER stress-inducible gene, is induced via ATF4-CHOP pathway and is involved in cell death. *EMBO J* 2005;24:1243–1255
 26. Ariyama H, Kono N, Matsuda S, Inoue T, Arai H. Decrease in membrane phospholipid unsaturation induces unfolded protein response. *J Biol Chem* 2010;285:22027–22035
 27. Mason P, Liang B, Li L, et al. SCD1 inhibition causes cancer cell death by depleting mono-unsaturated fatty acids. *PLoS One* 2012;7:e33823
 28. Fu S, Yang L, Li P, et al. Aberrant lipid metabolism disrupts calcium homeostasis causing liver endoplasmic reticulum stress in obesity. *Nature* 2011;473:528–531
 29. Volmer R, van der Ploeg K, Ron D. Membrane lipid saturation activates endoplasmic reticulum unfolded protein response transducers through their transmembrane domains. *Proc Natl Acad Sci USA* 2013;110:4628–4633
 30. Hayden MS, Ghosh S. Shared principles in NF- κ B signaling. *Cell* 2008;132:344–362
 31. Tanaka T, Tsujimura T, Takeda K, et al. Targeted disruption of ATF4 discloses its essential role in the formation of eye lens fibres. *Genes Cells* 1998;3:801–810
 32. Martinon F, Chen X, Lee AH, Glimcher LH. TLR activation of the transcription factor XBP1 regulates innate immune responses in macrophages. *Nat Immunol* 2010;11:411–418
 33. Boyce M, Bryant KF, Jousse C, et al. A selective inhibitor of eIF2 α dephosphorylation protects cells from ER stress. *Science* 2005;307:935–939
 34. Woo CW, Cui D, Arellano J, et al. Adaptive suppression of the ATF4-CHOP branch of the unfolded protein response by Toll-like receptor signalling. *Nat Cell Biol* 2009;11:1473–1480
 35. Jiang HY, Wek SA, McGrath BC, et al. Phosphorylation of the alpha subunit of eukaryotic initiation factor 2 is required for activation of NF- κ B in response to diverse cellular stresses. *Mol Cell Biol* 2003;23:5651–5663
 36. Lin YS, Green MR. Interaction of a common cellular transcription factor, ATF, with regulatory elements in both E1 α - and cyclic AMP-inducible promoters. *Proc Natl Acad Sci USA* 1988;85:3396–3400

ERK-Dependent Downregulation of Skp2 Reduces Myc Activity with HGF, Leading to Inhibition of Cell Proliferation through a Decrease in Id1 Expression

Xiaoran Li¹, Ying Bian¹, Yuri Takizawa^{1,2}, Tomio Hashimoto¹, Toshiyuki Ikoma³, Junzo Tanaka³, Naomi Kitamura¹, Yutaka Inagaki², Masayuki Komada¹, and Toshiaki Tanaka¹

Abstract

Hepatocyte growth factor (HGF) has an inhibitory effect on human HepG2 hepatoma cell proliferation. Previously, it was shown that HGF treatment downregulated Id1 and upregulated p16^{INK4a} in an ERK-dependent manner, leading to the inhibition of cellular proliferation. Here, new insight suggests that Skp2, an SCF complex component and potential prognosticator in cancer, is downregulated by injection of HGF into established HepG2 xenograft tumors. The downregulation was evident at both the mRNA and protein level and in an ERK-dependent manner. Critically, high expression of Skp2 restored HGF-inhibited cell proliferation, indicating that the inhibitory effect of HGF required the downregulation of Skp2. However, downregulation was not involved in the HGF-induced upregulation of a CDK inhibitor, p27^{Kip1}, a known SCF-Skp2 target. Instead, data revealed that Skp2 regulated Myc activity, which has oncogenic potential in the generation of hepatocellular carcinoma. Elevated expression of Skp2 or a mutant that is unable to associate with the SCF complex was capable of activating Myc, suggesting that Skp2 does not act on Myc as a component of the SCF complex, and thus functions as an activator of Myc independent of its role in ubiquitination. Furthermore, Skp2 regulated Id1 expression by regulating Myc activity, and the regulation of Skp2 is involved in the activity of p16 promoter through regulation of Id1 expression. Overall, these mechanistic findings provide the first evidence that ERK-dependent downregulation of Skp2 reduced Myc activity, leading to HGF-induced inhibition of cell proliferation through decreased Id1 expression.

Implications: This study elucidates the molecular details of HGF-induced inhibition of cellular proliferation in liver cancer cells. *Mol Cancer Res*; 1–11. ©2013 AACR.

Introduction

Hepatocyte growth factor (HGF) is a pleiotropic glycoprotein produced by stroma cells and associated with heparin in a wide variety of tissues. Its high affinity receptor c-Met is encoded by the *c-met* protooncogene and is widely expressed in epithelial cells (1). Binding of HGF activates the tyrosine kinase activity of c-Met, leading to cell proliferation, scattering, enhanced motility and so on, and thus HGF plays a key role in tumor–stroma interactions. Aberrant activation of c-Met, which can be induced through its mutation and/or

overexpression, causes many kinds of tumors (2). Recent efforts to find substances that inhibit the activation of c-Met are thus expected to lead to suppression of the malignant transformation of cells. However, HGF has an opposing effect on the regulation of cell proliferation in accordance with cell type: it promotes the proliferation of some tumor cells, but suppresses that of others (3, 4). This opposing effect is considered to depend on differences in the downstream pathways of c-Met (3–5). Thus, elucidation of the pathways responsible for the effect is expected to lead to new drugs for the suppression of tumor growth.

The binding of HGF to c-Met induces the phosphorylation of several tyrosine residues on c-Met followed by the recruitment of various signal transducers and adaptors such as Grb2 and Gab1, leading to activation of two major signaling pathways, the extracellular signal-regulated kinase (ERK), and phosphoinositide 3-kinase (PI3K)/Akt pathways (6, 7). We previously showed that HGF treatment of human HepG2 hepatoma cells inhibited cell proliferation by arresting the cell cycle at G₁ (8). This effect was overcome by partial inhibition of the ERK pathway with a low concentration of the MEK inhibitor PD98059, but not by inhibition of the PI3K pathway (7), showing that strong activation of ERK is essential for the inhibitory effect of HGF, but activation of the PI3K/Akt pathway is not. The strong

Authors' Affiliations: ¹Department of Biological Sciences, Graduate School of Bioscience and Biotechnology and ²Department of Regenerative Medicine, Tokai University School of Medicine, Isehara, Japan; ³Department of Inorganic Materials, Graduate School of Engineering, Tokyo Institute of Technology

Note: Supplementary data for this article are available at Molecular Cancer Research Online (<http://mcr.aacrjournals.org/>).

Corresponding Author: Toshiaki Tanaka, Department of Biological Sciences, Graduate School of Bioscience and Biotechnology, Tokyo Institute of Technology, 4259 Nagatsuta, Midori-ku, Yokohama, 226-8501, Japan. Phone: 81-45-924-5702; Fax: 81-45-924-5771; E-mail: ttanaka@bio.titech.ac.jp

doi: 10.1158/1541-7786.MCR-12-0718

©2013 American Association for Cancer Research.

activation of ERK by HGF upregulated expression of a Cdk inhibitor, p16^{Ink4a}, which led to a redistribution of other Cdk inhibitors, p21 and p27, from Cdk4 to Cdk2, resulting in low phosphorylation of pRb and G₁ arrest (8, 9). Because the upregulation of p16 expression is crucial to the G₁ arrest, we studied the mechanism responsible for it, and found that transcription factor Ets upregulates p16 through downregulation of a repressor protein for Ets, Id1 (10). The expression of Id1 is shown to be regulated at the transcription level (10), but the regulatory mechanism remains to be elucidated.

S-phase kinase-associated protein 2 (Skp2) is an F-box protein in the SCF complex, which consists of Skp1, Cullin, Rbx1 and an F-box protein (11), and is responsible for the ubiquitination and degradation of many kinds of proteins as an E3 ubiquitin ligase. F-box protein functions as the variable substrate-recognition component of the complex. More than 70 F-box proteins are present in the human genome and each is thought to have specific substrates and functions. Thus, the kinds and doses of F-box proteins define the functions of the SCF complex in cellular processes such as the cell cycle, signal transduction, and transcription. The SCF complex including Skp2 (SCF^{Skp2}) regulates G₁-S, the point responsible for defining the progression/arrest of a cell cycle, by regulating the degradation of substrates such as Cdk inhibitors (12). p27^{Kip1}, which induces cell-cycle arrest at G₁-S with inhibition of Cdk2/4/6, is a representative Cdk inhibitor suppressed by SCF^{Skp2} (13, 14). Overexpression of Skp2 leads to malignant progression of tumors through acceleration of p27 proteolysis (15, 16), implicating p27 in the function of Skp2 in tumor progression. In contrast, clinical research indicates the absence of an inverse correlation between Skp2 and p27 expression in some human sarcomas (17), suggesting that Skp2 has a p27-independent role in some cancer cells. In fact, a few reports have shown that Skp2 activates the transcription factor Myc through ubiquitination by SCF^{Skp2}, leading to upregulation of target genes involved in cell proliferation such as Cdc2 (18, 19). Also, a recent report showed that Skp2 upregulates expression of the *RhoA* gene, which has a role in cell invasion, by regulating Myc activity independently of the SCF complex (20). Hence, Skp2 seems to function as a regulator in tumorigenesis and cancer progression through various mechanisms.

We previously showed that HGF treatment of HepG2 hepatoma cells leads to suppression of cell proliferation through a redistribution of the Cdk inhibitors p21 and p27. Also, we showed that HGF treatment induces upregulation of p27 expression (9). In this study, we first examined the expression of Skp2, as the amount of p27 may be regulated via protein degradation with SCF^{Skp2}. We found that Skp2 expression is downregulated by injection of HGF into established tumors from HepG2 cells in mice. We conducted a detailed analysis of the role and mechanism of the downregulation with cultured HepG2 cells, and found that the downregulation occurs in an ERK-dependent manner at the mRNA and protein level, but this downregulation is not involved in the upregulation of p27 expression. We then examined the effect of the downregulation on the transcriptional activity of Myc, which has important roles

in hepatocarcinoma (21, 22). We found that the downregulation reduces Myc activity, and Skp2 functions as an activator of Myc independently of its role in ubiquitination. Finally, analysis of Id1, which is involved in the regulation of HepG2 cell proliferation, showed that the reduction in Myc activity caused by the Skp2 downregulation decreases Id1 expression, leading to activation of p16 promoter. We revealed in this study that the downregulation of Skp2 expression, which leads to a reduction in Myc activity, is crucial to the inhibitory effect of HGF on the proliferation of HepG2 hepatoma cells. Another hepatoma cell line, HuH7, proliferation of which is suppressed by HGF in an ERK-dependent manner, also showed ERK-dependent downregulation of Skp2 and Id1 suggesting that some cancer cells, other than HepG2 cells, arrest their proliferation by HGF in the same mechanism as HepG2 cells.

Materials and Methods

Cell culture

HepG2 cells and HuH7 cells were provided by Dr. S. Taketani and Dr. N. Kitamura, respectively, and have been described previously (7–10). Cells were cultured as previously described (9).

Reverse transcriptase-PCR

Total RNA was purified with ISOGEN (Nippon Gene) according to the manufacturer's instructions. cDNA synthesis was as described previously (10, 23). PCR was conducted with pairs of specific oligonucleotide primers (Skp2: 5'-CCTGTCTGTGCCTCCCTG-3' and 5'-CTGAGTG-ATAGGTGTTGG-3', p27^{Kip1}: 5'-ATGTCAAACGTGC-GAGTGTG-3' and 5'-ACGTTTGACGTCTTCTGAG-G-3'). p16^{Ink4a} and GAPDH were amplified with primers as described previously (9). PCR products were resolved on a 1.5% agarose gel and visualized with ethidium bromide staining.

Antibodies and immunoblotting

Detailed antibodies were described in Supplementary Data. Cell lysates were prepared as described previously (10). Equal amounts of protein in the precleared cell lysates (20–70 µg total protein) were resolved by SDS-PAGE on a 12% gel after heat denaturation. Immunoblotting was conducted as described previously (9, 24).

Established tumors originating from HepG2 cells

Nonobese diabetic/severe combined immunodeficiency (NOD/SCID) mice were purchased from Oriental Yeast Co., Ltd. Animal experiments were carried out in accordance with the institutional guidelines of Tokai University (Isehara, Japan). To deplete NK cells in the mice, 200 µL of 1 mg/mL anti-asialo GM1 antiserum (Wako Pure Chemical Industries, Ltd) was administered every 4 days. The mice were inoculated subcutaneously with 5 × 10⁶ HepG2 cells into the dorsal flanks. After establishment of tumors, HGF or PBS in a total volume of 200 µL was injected directly into the tumor tissues (100–130 mm²) for 7 consecutive days.

Tumor tissues were harvested after sacrifice of the mice and the lysates were prepared as described (10).

Construction of a Skp2 expression plasmid

Skp2 cDNA was amplified to construct a Skp2 expression plasmid with RT-PCR using a pair of oligonucleotide primers specific to the coding sequence of human Skp2 (forward 5'-ACACAAGCTTATGGATTACAAGGATGACGACGATAAGATGCACAGGAAGCACCTC-3', including a Flag tag sequence, and reverse 5'-ACACCTCGAGTCATAGACAACTGGGCTTTTGCAGTGT-CAG-3'). PCR amplification for constructing an expression plasmid for Skp2-LRR was done using another forward primer (5'-ACCAAGCTTATGGATTACAAGGATGACGACGATAAGTTAGACCTCACAGGTAA-3', including a Flag tag) and the reverse primer for human Skp2 described above. The PCR products were inserted into pcDNA3.1.

Secreted placental alkaline phosphatase (SEAP) reporter assay

A reporter construct, pMyc-SEAP (Clontech Laboratories, Inc), which contains several E-boxes at the 5' of the TATA-like promoter, was used to measure Myc activity, and a control construct containing only the basic TATA like promoter, pTAL-SEAP, was used as a negative control to measure activity of the basal TATA-like promoter. pMyc-SEAP or pTAL-SEAP was transfected into HepG2 cells with other expression plasmids. After 24 hours, the medium was replaced with fresh medium with or without HGF (50 ng/mL) in the absence or presence of PD98059. The cells were cultured for another 24 hours, and the medium was used for SEAP assays (Clontech Laboratories, Inc). To determine the net activity of SEAP, the activity in cells with the negative control (pTAL-SEAP) was used as a background value. All values were normalized with activity of β -gal, which was cotransfected with the reporter.

Silencing by siRNA

Synthetic siRNAs for Id1, Myc, and Skp2 were obtained from Integrated DNA Technologies, Inc. Detailed methods were described in Supplementary Data.

Luciferase reporter assays

The p16 promoter construct containing -247 to +1 from the transcription initiation site of the *p16* gene (kindly provided by Dr. E. Hara, Japan Foundation for Cancer Research, and described previously in ref. 9) was cotransfected with an expression plasmid for Skp2 and a standard amount of the pSV- β -galactosidase control plasmid (Promega). HGF treatment of the cells and luciferase reporter assays were conducted as previously described (9, 10).

Image manipulation

Adjustments of brightness and contrast with a linear algorithm were applied to the whole image.

Statistical analysis

The paired Student *t* test was used to test for significance where indicated.

Results

HGF downregulates Skp2 expression at the mRNA and protein level in an ERK-dependent manner

We found that injection of HGF into established tumors originating from HepG2 cells in NOD/SCID mice significantly downregulated Skp2 (Fig. 1A). Skp2 has transformation activity in experimental models, and is sometimes overexpressed in human cancers. To determine the role and mechanism of the downregulation of Skp2, we first conducted a time-course analysis of Skp2 expression in HepG2 cells treated with HGF. Western blot analysis showed that the level decreased for 24 hours, and remained low after 24 hours (Fig. 1B). As HGF treatment suppresses the proliferation of HepG2 cells through strong ERK activity (7, 9, 25), we examined the effect of ERK activity on the expression of Skp2. Treatment with a low concentration of PD98059, which partially inhibits ERK activity and restores cell proliferation suppressed by HGF (7, 9), restored the amount of Skp2 protein (Fig. 1B), indicating that Skp2 expression is regulated in an ERK-dependent manner, and suggesting the relevance of Skp2 to the regulation of cell proliferation. RT-PCR analysis showed that Skp2 mRNA expression was also downregulated by HGF and the amount of Skp2 mRNA was restored by a low concentration of PD98059 (Fig. 1C), showing that Skp2 expression is regulated at the transcription level in an ERK-dependent manner. HGF treatment of another hepatoma cell line, HuH7, proliferation of which is suppressed by HGF in an ERK-dependent manner (Supplementary Fig. S1), also led to ERK-dependent downregulation of Skp2 mRNA (Fig. 1D), suggesting that cancer cells other than HepG2 cells also are responsive to HGF.

To confirm that the strong ERK activity mediates the Skp2 downregulation, we used a HepG2 cell line, in which ERK activity is strongly activated by induction of active Ras (Ras V12) with Isopropyl- β -D(-)-thiogalactopyranoside (IPTG; ref. 7). Induction of the Ras, which suppressed proliferation of HepG2 cells, downregulated Skp2 (Fig. 1E), indicating that strong ERK activation is sufficient for downregulation of Skp2, and supporting that the expression of Skp2 is related to the regulation of proliferation in HepG2 cells.

Downregulation of Skp2 is not involved in the upregulation of p27, while it is involved in the suppression of cell proliferation with HGF

Figure 1B (left) shows that the timing of Skp2 downregulation after HGF treatment coincided with that of p27 upregulation. The expression of p27 mRNA was not altered by HGF (Supplementary Fig. S2), consistent with a report that p27 expression is regulated at the level of protein degradation via Skp2 (26). However, the partial inhibition of ERK activity with the low concentration of PD98059 had no effect on the upregulation of p27 by HGF, and p27 protein expression remained upregulated, even though the level of Skp2 protein was high (Fig. 1B, right). Moreover, with the HepG2 cell line, in which ERK is strongly activated by induction of active Ras with IPTG, we showed that activation of Ras did not alter the level of p27, while it

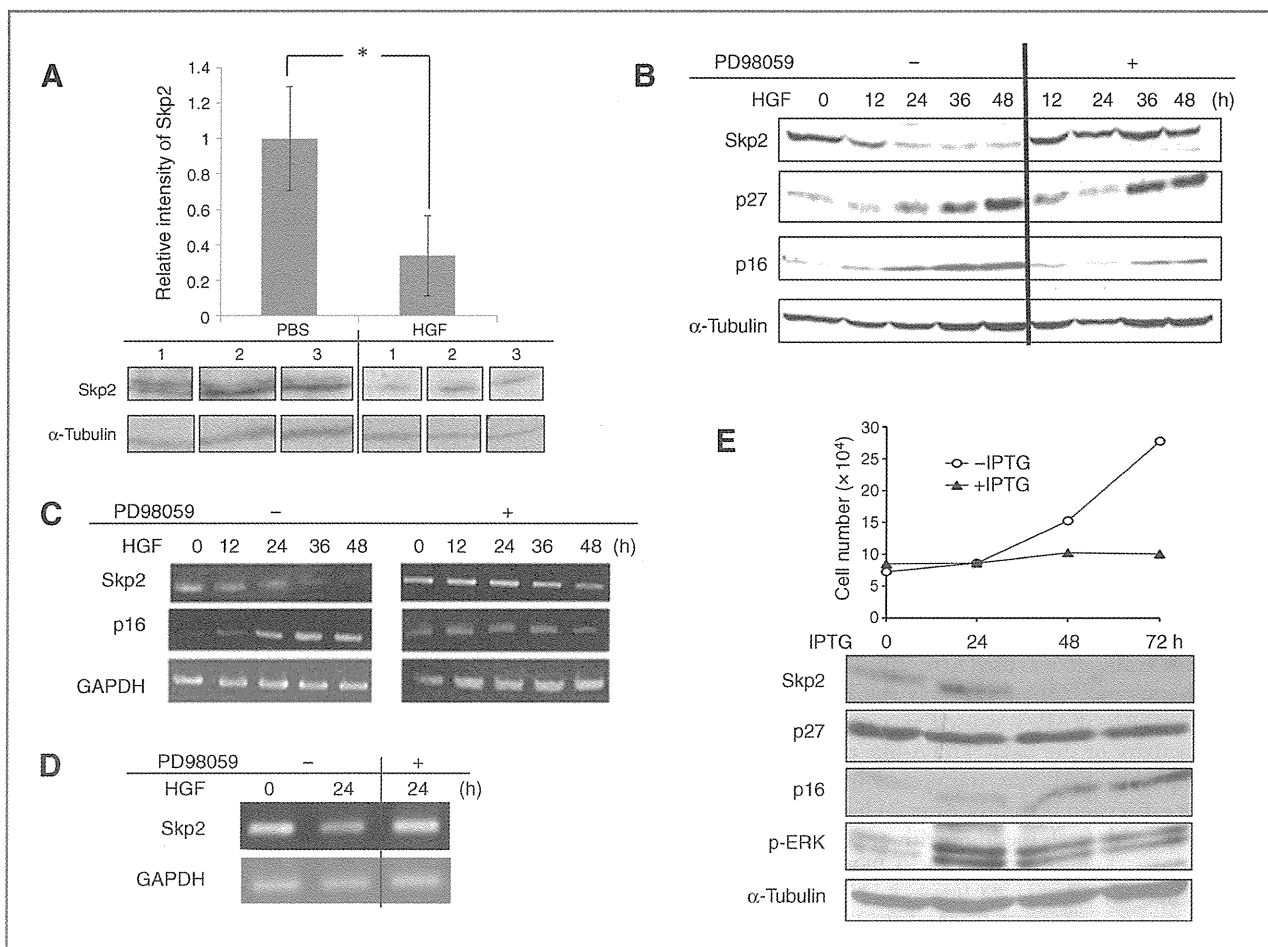


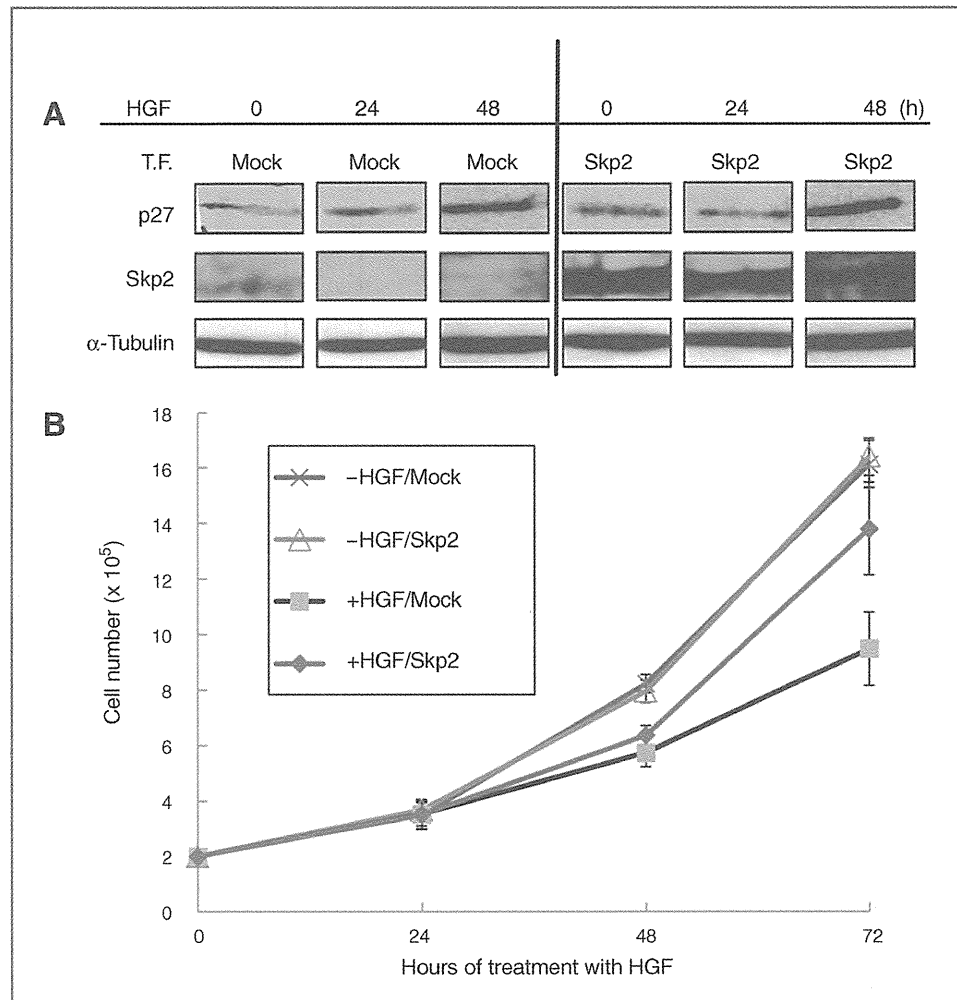
Figure 1. Skp2 is downregulated by HGF in an ERK-dependent manner. **A**, Western blot analysis to detect Skp2 in established tumors from HepG2 cells in NOD/SCID mice. All bands in analysis with anti-Skp2 and α -tubulin antibodies, respectively, were acquired from a single film exposure. Unprocessed full-length blots are presented in Supplementary Fig. S4. The intensity of the band in the bottom was quantitated using NIH ImageJ software and graphed. Each value represents the mean \pm S.D. ($n = 3$). *, $P < 0.05$; Student t test. **B**, Western blot analysis to detect Skp2 and p27 in HepG2 cells treated with HGF in the absence (–) or presence (+) of PD98059. Cell lysates were prepared at the indicated times (h) after HGF treatment and subjected to Western blot analysis. Tubulin was used as a loading control. p16 is shown to assess the effect of HGF. The result is representative of three independent experiments. **C**, RT-PCR analysis of Skp2 in HepG2 cells treated with HGF in the absence (–) or presence (+) of PD98059. Total RNA was purified at the indicated times and subjected to RT-PCR. GAPDH was used as an internal control. p16 is shown to assess the effect of HGF. The result is representative of two independent experiments. **D**, RT-PCR analysis of Skp2 in HuH7 cells treated with or without HGF for 24 hours in the absence (–) or presence (+) of PD98059. Total RNA was purified and subjected to RT-PCR. GAPDH was used as an internal control. **E**, time course analysis of cell proliferation (top) and Western blot analysis to detect Skp2 and p27 in cells with forced activation of ERK (bottom). After the active form of Ras was induced with IPTG, cell numbers were counted and cell lysates were prepared at the indicated times after induction. Phospho-ERK and p16 are shown to assess the effect of Ras induction. Experiments were done twice with similar results, and representative data are shown.

downregulated Skp2 expression (Fig. 1E). These results suggested that the downregulation of Skp2 is not involved in the upregulation of p27. They also showed that the upregulation of p27 by HGF is not mediated by the ERK activity, and suggested that the upregulation is not involved in the inhibitory effect of HGF on HepG2 cell proliferation.

To directly show that the downregulation of Skp2 is not involved in the upregulation of p27, experiments with high expression of Skp2 were conducted. HepG2 cells were transfected with Skp2, and the protein levels of Skp2 and p27 were examined by Western blot analysis after HGF treatment. High expression of Skp2 did not suppress the upregulation of p27 (Fig. 2A), showing the upregulation to

be independent of the downregulation of Skp2. In contrast, cell counts showed that high expression of Skp2 restored the cell proliferation suppressed by HGF (Fig. 2B), indicating that downregulation of Skp2 is essential for the inhibitory effect of HGF on the proliferation of the cells. The data also suggested that the upregulation of p27 is not involved in the inhibitory effect of HGF, as high expression of Skp2 did not suppress the upregulation (Fig. 2A). Although the number of cells was restored with high expression of Skp2 in the presence of HGF, it did not reach the number achieved in the absence of HGF (Fig. 2B). This may simply be due to the transfection efficiency of the construct to express Skp2.

Figure 2. High expression of Skp2 has no effect on p27, but restores cell proliferation suppressed with HGF. A, Western blot analysis to detect p27 in cells with high expression of Skp2. All bands in analysis with anti-p27, Skp2, and α -tubulin antibodies, respectively, were acquired from a single film exposure. Full-length blots are presented in Supplementary Fig. S5. B, time course analysis of proliferation in cells transfected with Skp2 in the absence or presence of HGF. Cells were prepared as described in (A) and cell numbers were counted at the indicated times. Each value represents the mean \pm S.D. of triplicate determinants. The results are representative of three independent experiments.



Downregulation of Skp2 with HGF reduces Myc activity

A few reports have indicated that Skp2 has another role in activation of the transcription factor Myc (18, 19), and Myc was reported to have important roles in hepatocarcinoma (21, 22). A recent report showed that knockdown of Myc suppressed proliferation of HepG2 cells (27), and we obtained results consistent with this by knockdown of Myc (data not shown), indicating that Myc expression is required for the proliferation of HepG2 cells. Thus, we studied the relevance of Skp2 to Myc in HepG2 hepatoma cells. We first examined Myc activity in HepG2 cells treated with HGF. A promoter-reporter construct, in which the SEAP reporter gene is regulated by binding of Myc on the promoter, was introduced into the cells, and the SEAP activity was analyzed in the absence or presence of HGF with or without the low concentration of PD98059. HGF treatment of the cells greatly reduced endogenous Myc activity, and the partial inhibition of ERK activity with PD98059 significantly restored the Myc activity suppressed by HGF (Fig. 3A), indicating that the Myc activity is regulated by HGF in an ERK-dependent manner. To know which Myc family proteins are involved in the Myc activity in HepG2 cells,

we examined the levels of c-myc, N-myc, and L-myc by RT-PCR. The expression of c-myc was much higher than that of the others (data not shown). Thus, the Myc activity seems to be mostly derived from c-Myc in the cells.

As the Myc protein is known to be unstable (28), it is possible that the inactivation of Myc with HGF simply reflects loss of the protein. However, Western blot analysis showed that the amount of c-Myc is not altered in the presence of HGF (Fig. 3B), suggesting that the reduction in Myc activity with HGF is not caused by loss of the protein. We also analyzed the levels of Max and Mad, because in the Myc/Max/Mad network, the association of Myc with Max leads to transcriptional activation, and that of Mad with Max to repression (29). We did not detect any changes in their expressions in HepG2 cells treated with HGF (Supplementary Fig. S3), suggesting that the reduction in Myc activity by HGF is not regulated by changes in the amounts of Mad and Max.

As the reduction in Myc activity by HGF is mediated through the strong ERK activity, it may be caused by the downregulation of Skp2. We thus examined whether Skp2 regulates endogenous Myc activity. We introduced the

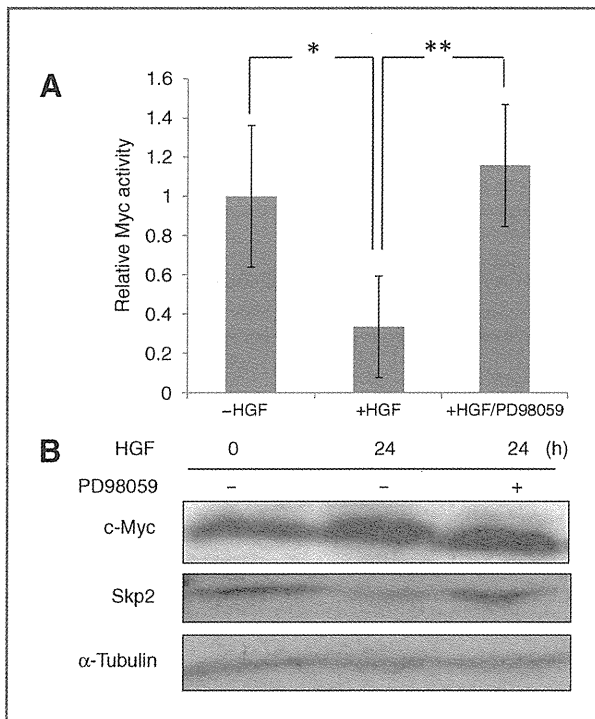


Figure 3. HGF treatment reduces Myc activity, but does not alter the amount of c-Myc. **A**, detection of endogenous Myc activity in cells treated with HGF in the absence or presence of PD98059. All values were normalized as described in Materials and Methods. The average fold-increase in Myc activity compared with activity in the absence of HGF without PD98059 is indicated. Each value represents the mean \pm S.D. of triplicate determinants from a representative experiment. *, $P < 0.05$; **, $P < 0.01$, Student *t* test. **B**, Western blot analysis to detect c-Myc. Cells were treated with HGF in the absence or presence of PD98059 and cell lysates were prepared at 0 or 24 hours. Skp2 is shown to assess the effect of HGF or HGF plus PD98059. Experiments were carried out twice with similar results, and representative data are shown.

reporter for Myc together with the construct to express Skp2 into the cells. High expression of Skp2 activated Myc activity in the absence or presence of HGF (Fig. 4A), indicating that Skp2 is sufficient to activate endogenous Myc. Next, to directly show that the reduction in Myc activity is caused by the downregulation of Skp2, we introduced Skp2 siRNA into the cells. Knockdown of Skp2 significantly decreased endogenous Myc activity without altering the amount of c-Myc in the absence of HGF (Fig. 4B and C), indicating that Skp2 is essential to activate Myc in proliferating cells. These results showed that Skp2 functions to activate Myc, and thus, downregulation of Skp2 results in the reduction in Myc activity.

Myc activity is regulated by Skp2, but not through SCF^{Skp2}

It was previously shown that Myc is activated via ubiquitination by the SCF complex including Skp2 (SCF^{Skp2}). The ubiquitination results in rapid degradation of Myc (18, 19). However, inhibition of ubiquitination and degradation with knockdown of Skp2 induced no accumulation of Myc

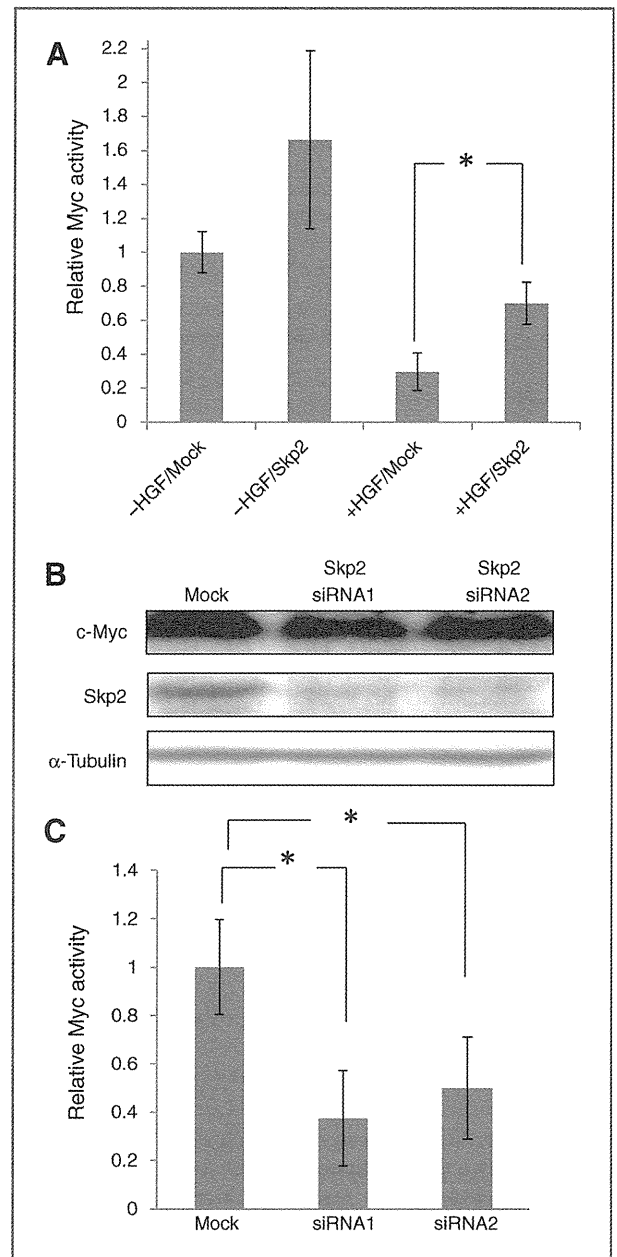


Figure 4. Skp2 is involved in regulation of endogenous Myc activity. **A**, detection of endogenous Myc activity in cells with high expression of Skp2. The average fold-increase in SEAP activity compared with activity in the absence of HGF with a Mock-transfection is indicated. Each value represents the mean \pm S.D. of triplicate determinants from a representative experiment. *, $P < 0.01$; Student *t* test. **B**, Western blot analysis to detect c-Myc in cells with Skp2 knockdown. Cells were transfected with two kinds of siRNA targeting Skp2 or randomized siRNA (Mock) as a control. Cell lysates were prepared at 24 hours after transfection and subjected to immunoblotting. Experiments were carried out twice with similar results and representative data are shown. **C**, detection of endogenous Myc activity in cells with Skp2 knockdown. The average fold-decrease in Myc activity compared with a Mock transfection is indicated. Each value represents the mean \pm S.D. of triplicate determinants from a representative experiment. *, $P < 0.001$; Student *t* test.

protein (Fig. 4B), suggesting that ubiquitination of Myc by SCF^{Skp2} is not involved in the regulation of Myc activity. To directly show whether or not the SCF complex is required for the transcriptional activation of Myc by Skp2, we adopted a mutant of Skp2, Skp2-leucine-rich repeats (LRR), which has a deletion in the N-terminus including a part of the F-box domain, resulting in an inability to couple to the SCF complex (18). High expression of not only the wild-type Skp2 but also Skp2-LRR restored the Myc activity reduced by HGF treatment (Fig. 5A), indicating that Skp2 regulates Myc activity, but ubiquitination of Myc by the SCF complex is not involved in the regulation of Myc activity by Skp2. This idea was supported by the finding that high expression of Skp2 and Skp2-LRR did not change the amount of Myc protein (Fig. 5B).

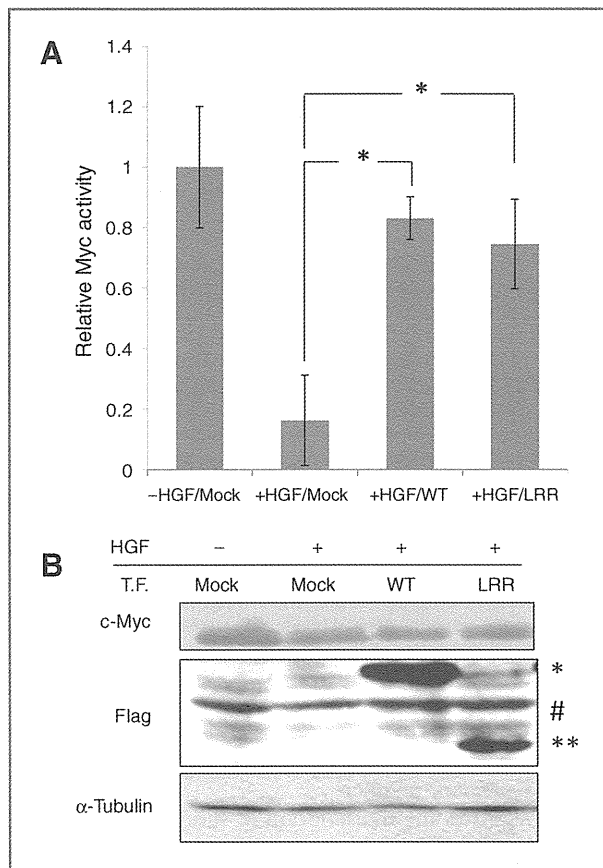


Figure 5. High expression of Skp2-LRR restores Myc activity suppressed by HGF. A, detection of endogenous Myc activity in cells with high expression of Skp2 (WT) or Skp2-LRR (LRR). The average fold-decrease in Myc activity compared with activity in the absence of HGF with a Mock transfection is indicated. Each value represents the mean \pm S.D. of triplicate determinants from a representative experiment.

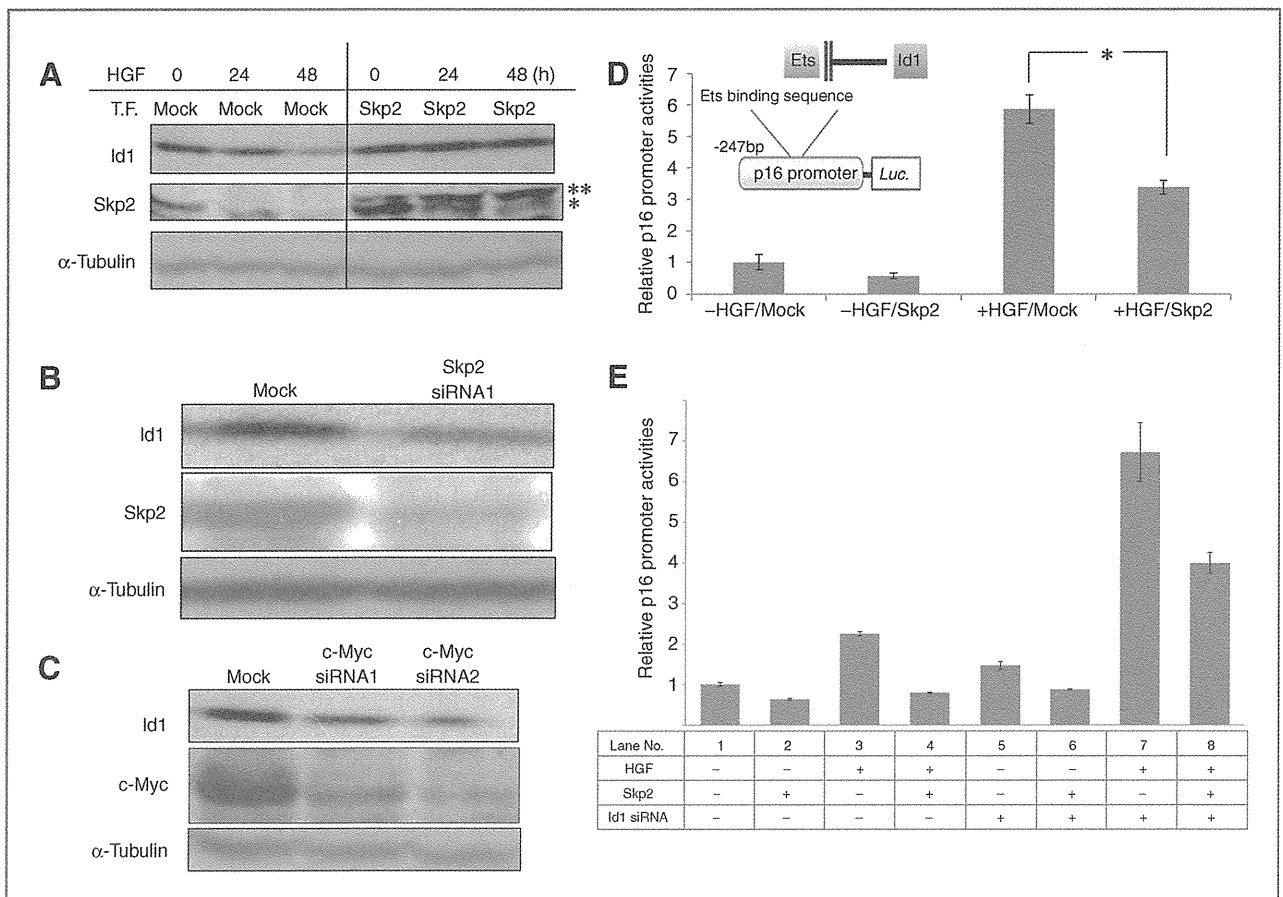
*, $P < 0.01$; Student *t* test. B, Western blot analysis to detect c-Myc in cells transfected with Skp2 (WT) or Skp2-LRR (LRR). Exogenous Skp2 and Sk2-LRR were detected with anti-Flag and their positions are indicated with * and **, respectively. The signal represented by # is nonspecific. Experiments were carried out twice with similar results and representative data are shown.

Skp2 is involved in Id1 expression through regulation of Myc activity

Myc regulates transcription of a wide range of genes responsible for regulation of cell proliferation, transcription, cell motility and so on (29). To uncover the target of Myc activated by Skp2 in the hepatoma cells, and to address the mechanism by which Skp2 affects proliferation through HGF signaling, we focused on a transcriptional regulator, Id1: Id1 seemed to be a target of Myc activated by Skp2, because our previous study showed that Id1, whose the mRNA and protein are downregulated by HGF, is involved in the anti-proliferative effect of HGF through regulation of p16 expression (10), and it was recently reported that c-Myc upregulated Id1 expression in human breast cancer cells and prostate cancer cells (30, 31). In addition, Id1 expression in another hepatoma cell line, HuH7, proliferation of which is suppressed by HGF in an ERK-dependent manner (Supplementary Fig. S1), was also regulated in an ERK-dependent manner (Supplementary Fig. S6), suggesting that Id1 is involved in the inhibitory effect of HGF on proliferation of cancer cells other than HepG2. Western blot analysis showed that high expression of Skp2 restored the expression of Id1 suppressed by HGF (Fig. 6A), and knockdown of Skp2 suppressed the expression of Id1 in the absence of HGF (Fig. 6B and Supplementary Fig. S7), showing that Skp2 is involved in the regulation of Id1 expression. In addition, knockdown of Myc suppressed the expression of Id1 in the absence of HGF (Fig. 6C), indicating that Myc regulates Id1 expression. These results, together with the fact that Skp2 regulates Myc activity, suggest that Skp2 regulates Id1 expression through the regulation of Myc activity. Also, high expression of the Skp2 mutant, Skp2-LRR, restored Id1 expression and cell proliferation suppressed by HGF (Supplementary Fig. S8), suggesting that Id1 expression is regulated by Skp2 in the SCF complex-independent manner. As we previously showed that the downregulation of Id1 results in the activation of the promoter of the *p16* gene (10), we next examined the effect of Skp2 on the promoter. A promoter-reporter construct, in which expression of luciferase is regulated by a minimal promoter of the *p16* gene (9), was introduced into HepG2 cells together with the construct to express Skp2 in the absence or presence of HGF. While HGF treatment of the cells activated the p16 promoter as previously reported (9), high expression of Skp2 significantly suppressed the activation of the p16 promoter (Fig. 6D). Also, knockdown of Id1 restored the promoter activity suppressed by high expression of Skp2 in the presence of HGF (Fig. 6E, lane 3, 4, and 8). These results supported that Skp2 regulates Id1 expression, leading to regulation of p16 promoter. Higher activity of p16 promoter induced by Id1 siRNA (lane 7 and 8) than that induced by randomized siRNA (lane 3 and 4) in the presence of HGF seems to represent a partial reduction, but not complete elimination, of Id1 by HGF treatment of the cells.

Discussion

Recent clinical research suggests that Skp2 has a p27-independent role in some cancer cells (17). In this study, we



reported that ERK-dependent downregulation of endogenous Skp2 by HGF reduces Myc activity, leading to inhibition of HepG2 hepatoma cell proliferation through a decrease in Id1 expression. The downregulation was also confirmed in established tumors from HepG2 cells in mice. Our data reveal a mechanism by which HGF suppresses cell proliferation through Skp2 downregulation. Our data suggested that Skp2 is physiologically involved in the regulation of Myc activity as its activator independently of its role in ubiquitination, but not in the regulation of p27 degradation. In addition, a hepatoma cell line other than HepG2, HuH7, proliferation of which is also suppressed by HGF in an ERK-dependent manner, also showed ERK-dependent downregulation of Skp2 (Fig. 1D) and Id1 (Supplementary Fig. S6), suggesting that some other cancer cells arrest their

proliferation by HGF through Skp2 downregulation in the SCF-independent manner.

Myc regulates the transcription of various genes responsible for controlling cell proliferation, the cell cycle, transcription, cell motility and so on, leading to the initiation, promotion, and progression of a wide range of cancers (32). Among the targets of Myc, we found in this study that expression of Id1 is regulated by Myc through Skp2 (Fig. 6). A comprehensive analysis to find Myc-binding sites in a human genome with ChIP assays showed a binding site in the upstream region of the *Id1* gene (33), supporting regulation of Id1 expression by Myc through Skp2. As we previously showed that Id1 is downregulated by HGF (10), which leads to inhibition of HepG2 cell proliferation, we propose the model displayed in Fig. 7 to illustrate the